RESEARCH ARTICLE





Fusion of Multispectral and Panchromatic Images by Integrating Standard PCA with Rotated Wavelet Transform

Rishikesh G. Tambe¹ • Sanjay N. Talbar² • Satishkumar S. Chavan³

Received: 1 April 2020 / Accepted: 16 April 2021 © Indian Society of Remote Sensing 2021

Abstract

Many pansharpening algorithms are based on the principle of extracting spatial details from panchromatic (PAN) images and injecting them into multispectral (MS) images. In this paper, we present two fusion approach based on same principle by integrating standard principle component analysis (PCA) with decimated and undecimated rotated wavelet transform. When decimated/subsampled rotated wavelet transform (SSRWT) is used for fusion of MS and PAN images, three visual artifacts get introduced in the fused image namely color distortion, shifting effect and shift distortion. To eliminate color distortion, SSRWT is integrated with standard PCA, i.e., PCA-SSRWT. Color distortion is significantly mitigated, but shifting effect and shift distortion persist in the fused image of PCA-SSRWT. After employing undecimated/nonsubsampled rotated wavelet transform (NSRWT), shifting effect and shift distortion get eliminated with minimum color distortion. However, fused image as a result of NSRWT is spectrally high but spatially low. In order to improve spatial quality and remove visual artifacts observed in SSRWT and PCA-SSRWT, NSRWT is integrated with standard PCA, i.e., PCA-NSRWT. Visual and quantitative analysis is carried out to validate the quality of fused image for all the algorithms. Visual interpretation suggests that fused image obtained using PCA-NSRWT is superior to fused images of SSRWT, PCA and NSRWT. The overall quantitative analysis manifests that the PCA-NSRWT is consistent with visual interpretation and performs better than state-of-the-art methods. PCA-NSRWT not only removes visual artifacts but also improves spectral and spatial quality of the fused image compared to individual PCA, SSRWT, NSRWT and PCA-SSRWT. Based on visual and quantitative analysis, it is observed that PCA works better with undecimated compared to decimated rotated wavelet transform for fusion.

Keywords Nonsubsampled rotated wavelet transform (NSRWT) \cdot Principal component analysis (PCA) \cdot Satellite image fusion \cdot Shift distortion \cdot Shifting effect \cdot Subsampled rotated wavelet transform (SSRWT)

☐ Rishikesh G. Tambe rishitambe@gmail.com

Published online: 27 April 2021

Introduction

Remote sensing plays a significant role in examining surface of earth through images captured by sensors on board of satellite. Sensors have specific objectives as different sensors are characterized to record various features about earth's surface (Pohl & Van Genderen, 2016). Based on objective of sensors, they have different spectral, spatial resolution and information content is reciprocal to each other. Many earth observation satellites such as QuickBird, WorldView-3, Pleiades-1A, IKONOS, SPOT-5, LAND-SAT-8 provide spectral information at resolution of 1.24–30 m through several MS bands and spatial information at resolution of 0.5–15 m using single PAN band. However, no sensor provides information which is



Department of Computer Science and Engineering, SGGS Institute of Engineering and Technology, Nanded, Maharashtra 431606, India

Department of Electronics and Telecommunication Engineering, SGGS Institute of Engineering and Technology, Nanded, Maharashtra 431606, India

Department of Electronics and Telecommunication Engineering, Don Bosco Institute of Technology, Kurla (W), Mumbai, Maharashtra 400070, India

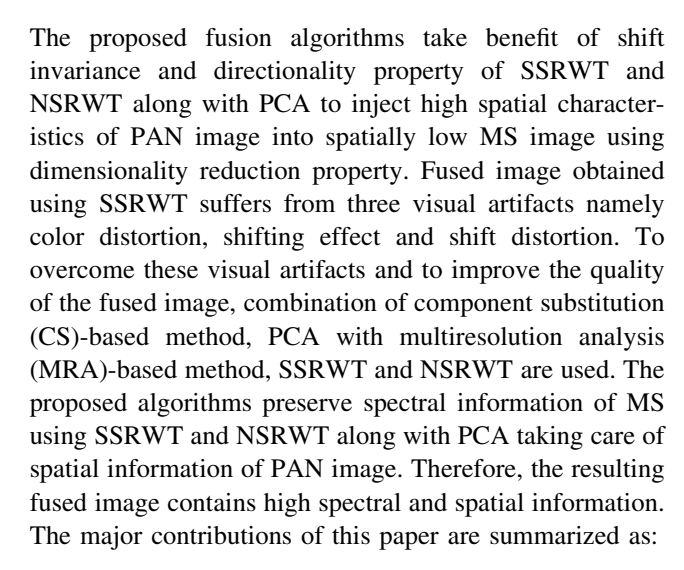
spectrally as well as spatially high at once due to limitation of sensor technology.

High spectral and spatial information is desirable for many applications. Applications such as land-use or land-cover in which spectral information is of more importance, while high spatial information is more suited for applications such as object recognition and to identify various features and structures in urban study. A single image either with high spectral or spatial information cannot meet the needs of various applications. Therefore, it is obligatory to combine the spectral and spatial information for such applications.

To combine the high spectral and spatial information, image fusion is a promising pre-processing tool for many applications. According to Pohl and Van Genderen (1998), image fusion is a process of combining complementary information from two or more images into a single fused image. However, the definition does not deal with the quality of the fused image (Wald, 1999). Mangolini (1994) focused not only on combining two or more images but also on the quality of the fused image. Hence, it is imperative to not only combine but also improve the spectral and spatial quality of fused image. In general, MS imaging sensors record information which is spectrally high and spatially low whereas PAN imaging sensors record information which is spectrally low but spatially high. High spectral content of MS image can be combined with high spatial content of PAN image to get the fused image which is superior in quality to individual MS and PAN images (Mangolini, 1994). When this fusion is performed using MS and PAN images, it is popularly known as pansharpening.

Pansharpening can be considered as special case of image fusion. Many pansharpening methods have been proposed by several researchers and still coping with improving spectral and spatial quality of the fused image. Most of the state-of-the-art fusion methods give good result but still lack in preserving spectral quality due to variations in gray values between MS and PAN images. Recently, fusion algorithm based on Bayesian-based methods, sparse representation/reconstruction has been proposed (Vicinanza et al., 2015). Even though these fusion algorithms show promising results, they are unable to find their ways in becoming practically operational due to their complex architecture and are computationally expensive. Traditional pansharpening algorithms are well reviewed and tested, so many researchers are still focusing on the state-of-the-art pansharpening methods for enhancing spectral and spatial quality of the fused image. So to achieve better quality of the fused image, many researchers proposed several hybrid pansharpening algorithms.

In this paper, two hybrid satellite image fusion methods are proposed namely PCA-SSRWT and PCA-NSRWT.



- Color distortion observed in the fused image of SSRWT is alleviated by a new hybrid pansharpening algorithm, PCA-SSRWT.
- Visual artifacts namely shifting effect and shift distortion are noticed in SSRWT, and PCA-SSRWT are addressed by second hybrid pansharpening algorithm, PCA-NSRWT. It not only eliminates these artifacts but also improves spectral and spatial quality of the resultant fused image.

The remainder of this paper is organized as follows. "Related Work" section deals with literature survey of fusion algorithms for satellite images. In "Standard PCA" and "Subsampled Rotated Wavelet Transform (SSRWT)" sections, standard PCA and rotated wavelet transform are reviewed, respectively. In "Proposed Fusion Algorithms" section, the proposed hybrid algorithms for satellite image fusion are presented. "Result and Discussion" section comments on experimental results and analysis of different algorithms using fusion metrics. Concluding remarks are reported in "Conclusion" section.

Related Work

Several researchers have proposed pansharpening algorithms using different mathematical tools for various applications such as urban classification, change detection. (Pohl & Van Genderen, 2016). A comparative study of pansharpening algorithms has been reviewed by Pohl and Van Genderen (2016), Vivone et al. (2015), Aiazzi et al. (2012). Many researchers have tried to classify pansharpening algorithms into various classes (Zhang & Huang, 2015). The two major approaches which are widely used in satellite image fusion are CS and MRA. The first approach depends on substitution of a component of MS image by high spatial PAN image. Many researchers have proposed



fusion algorithms based on image transformation which include intensity-hue-saturation (IHS) (Carper et al., 1990), Gram–Schmidt transform (GST) (Laben & Brower, 2000), adaptive GS (Garzelli et al., 2008), PCA (Shah et al., 2008), etc. Algorithms belonging to this class are straightforward, less complicated and easy to implement. However, the fused images as a result of CS-based methods are visually attractive but are spectrally distorted.

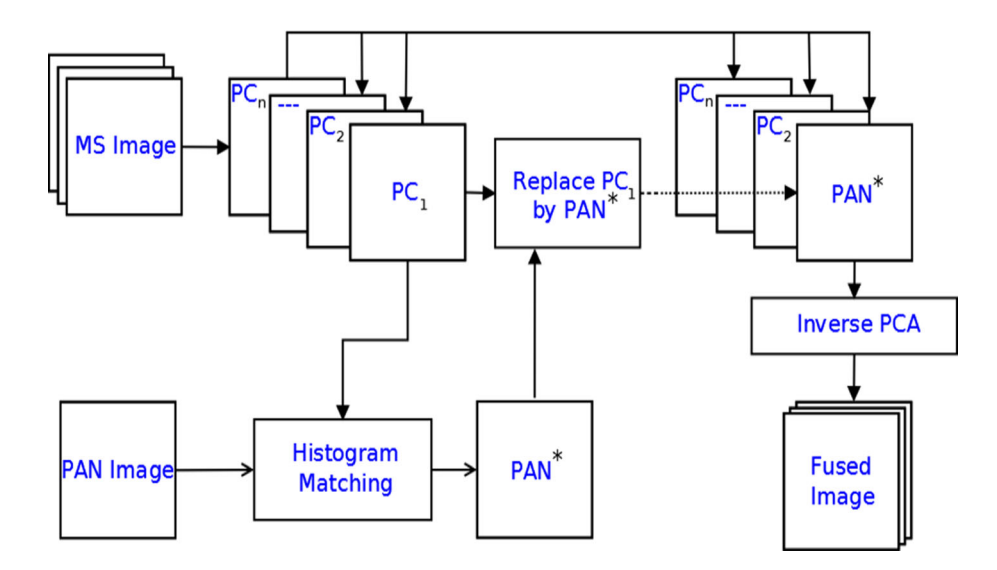
In the second approach, input images are decomposed at different scales followed by feature extraction from PAN image and MS image. Fused images obtained using MRAbased methods provide spectral as well as spatial information simultaneously. For instance, wavelet-based fusion algorithms (Aiazzi et al., 2002; Amolins et al., 2007; Nunez et al., 1999) and pyramid-based fusion methods (Burt & Adelson, 1983) belong to class of MRA fusion algorithms and both of them have their own advantages and disadvantages. Fused image obtained by pyramid fusion algorithm includes extraneous edge information and originates blocking artifacts as number of decomposition levels increases. Treating these as a major concern, researchers are exploring wavelet-based fusion techniques for the last two decades. Fusion algorithm based on wavelet includes discrete wavelet transform (DWT) which preserves spectral as well as spatial information but is shift variant and has poor directionality (Li et al., 1995; Mallat, 1989). To overcome the limitations of DWT, stationary wavelet transform (SWT) was proposed in Nason and Silverman (1995), where decomposition was performed without subsampling. SWT is computationally expensive than DWT as it is influenced by number of decomposition levels (Pradhan et al., 2006). Kingsbury (1999) proposed dual-tree complex wavelet transform (DT-CWT) which is shift invariant, computationally efficient and has better directionality property. The contourlet transform (CT) (Do & Vetterli, 2005) is a multiscale and multidirectional transform where point discontinuities are captured by Laplacian pyramid (LP) (Burt & Adelson, 1983) followed by use of directional filter bank (DFB) (Bamberger & Smith, 1992) to link point discontinuities into linear structure. However, subsampling process in both LP and DFB makes the CT shift variant which results in ringing artifacts. To overcome problem of CT, Da Cunha et al. (2006) proposed NSCT which is shift invariant, multiscale and multidirectional framework. Pansharpening performed using NSCT shows good results by preserving spectral features by compromising spatial quality of the fused image. Computational complexity of NSCT is high as compared to other waveletbased fusion methods. To eliminate the computational burden and increase the number of directional information, the shearlet transform (ST) was proposed Labate et al. (2005). ST working can be divided into two phases: pyramid filter banks (PFB) and shearing filter banks (SFB).

ST lacks shift-invariance due to subsampling operation in both PFB and SFB. Easley et al. (2008) proposed non-subsampling shearlet transform (NSST) which omits sampling operation. NSST has shown good fusion result with low computational burden. However, designing good filter for the NSST is a challenging task. These methods show promising experimental results, but excess computational burden restricts them from practical usage.

Many authors have tried to overcome the drawbacks of one fusion approach by taking benefit of other approach through integrating two fusion methods. Ehlers et al. (2010) presented pansharpening algorithm which is based on IHS and fast Fourier transform (FFT). IHS transform is used to transform MS bands into IHS space followed by FFT applied to intensity component and PAN image. Then, inverse FFT followed by inverse IHS is performed to get the fused image. Even though this method works for fusing multi-sensor and multi-temporal images, the power spectrum is used to design the high-pass filter for PAN image and low-pass filter for intensity component of MS image. The cut-off frequency for these filters has to be established explicitly which makes the process complex. Chibani and Houacine (2002) proposed hybrid satellite fusion method based on IHS and redundant wavelet algorithm (WIHS). Though WIHS preserves spectral information due to use of redundant wavelet algorithm but fails in capturing spatial information which is less than what IHS alone obtains. Zhang and Hong (2005) proposed fusion technique based on integration of IHS and non-redundant wavelet algorithm which shows promising results but still the fused image is spectrally distorted and information is lost due to use of decimated wavelet algorithm. González-Audícana et al. (2004) proposed a hybrid pansharpening fusion algorithm by using improved IHS and PCA for extracting spatial details from PAN image and later injected into individual MS bands which are decomposed using Mallat's subsampled and nonsubsampled wavelet algorithms (Mallat, 1989). Here, nonsubsampled wavelet algorithm showed better results with IHS and PCA than subsampled algorithm. Johnson et al. (2013) proposed hybrid fusion algorithm by integrating IHS and smoothing filter intensity modulation (SFIM) as a pre-processing for image classification. The window size of smoothing filter which is used for averaging neighboring pixels of PAN image depends on spatial ratio of MS and PAN images. As spatial ratio decreases, the quality of fused image decreases (Ling et al., 2008). Zhong et al. (2017) proposed generalized band-dependant spatial-detail (GBDSD) algorithm which is combination of CS and MRA-based methods. Though computationally less expensive, the fused image obtained from GBDSD is spectrally high but fails at inheriting spatial quality. Recently, Faragallah (2018) presented pansharpening algorithm which combined adaptive PCA



Fig. 1 Block schematic for satellite image fusion using PCA



(APCA) and high-pass modulation (HPM) for fusion of MS and PAN images. To resolve the window size and standard deviation of Gaussian low pass filter (GLPF) which is used for smoothing PAN image, the proposed pansharpening algorithm is adjusted with multi-objective optimization (MOO). The method depends on window size of filter which is determined by spatial ratio of the MS and PAN images. For single-sensor, the method works well but for multi-sensor satellite image fusion, it may not work as spatial ratio varies from sensor to sensor. If spatial ratio is small enough, the spectral quality of the fused image may increase by compromising spatial information (Ling et al., 2008). Zhang et al. (2019) proposed image fusion-based method using spatial weighted neighbor embedding (SWNE). The fused image generated is spatially high but fails to preserve spectral characteristics from MS image. Recently, many image fusion and pan-sharpening algorithms have been proposed due to advancement in sensor technology and demand of image representation and analysis (Liu et al., 2018; Ma et al., 2020; Masi et al., 2016; Xu et al., 2020; Yang et al., 2017). All the convolutional neural network (CNN)-based pan-sharpening methods (Liu et al., 2018; Ma et al., 2020; Masi et al., 2016; Xu et al., 2020) show good result but at the cost of high computational complexity. Further, CNN-based image fusion methods require huge amount of data along with ground truth for training purpose (Ma et al., 2019).

All of the above methods have some advantages and limitations over each other, but still there is a lot of room for improving spectral as well as spatial characteristics of the fused image.

Standard PCA

Standard PCA is also known as Karhunen–Loève (KL) and Hotelling transform which is mathematical transformation to produce new images called as components or axes. PCA alters input MS bands into new rotated axes which are orthogonal in nature to other axes. Mathematically, there is no correlation among newly generated components. Initially, transformation employs eigenvalues and vectors from correlation matrix of MS image to obtain principal components. The newly generated principal components carry and reconstruct most of the information from input images. Block schematic of PCA for merging MS and PAN image is shown in Fig. 1.

The covariance matrix represents variances and covariance present in all the MS bands. Out of total variances of the input image, maximum fraction of variance is mapped in PC₁ and can be calculated by Eq. 1, where σ_X^2 is variance, μ_X is the mean representing gray values of image band X and can be computed using Eq. 2. Pixel is denoted by X_i for k number of pixels.

$$\sigma_X^2 = \frac{\sum_{j=1}^k (X_j - \mu_X)^2}{k - 1} \tag{1}$$

$$\mu_X = \frac{\sum_{j=1}^k X_j}{k}.\tag{2}$$

The correlation represents the trade-off between gray values of the pixel throughout various bands with respect to the means of their corresponding bands. The correlation $CR_{(X,Y)}$ between gray values of different bands can be calculated using Eq. 3. Here, X and Y denote gray values of two different bands at pixel j out of k number of pixels, μ_X and μ_Y are means for X and Y bands of images, respectively (Aiazzi et al., 2012; Pohl & Van Genderen, 2016).



Fig. 2 Two-level decomposition Second Level using 2D SSRWT H_{R(O)} First Level $H^{\overline{AD}}$ $I_{\frac{m}{2}}^{AA} \times \frac{n}{2}$ R(O) $^{1}R(\Theta)$ H_{R(θ)} $\hat{I}_{\frac{m}{4}X^{-}}^{DD}$ H_{R(θ)} F(x,y)_{m×n} $H_{R(\Theta)}^{DD}$ $H_{R(\boldsymbol{\theta})}^{DA}$ H^{DD} $R(\Theta)$ ↑ f_y • f_y

Fig. 3 Fourier spectrum a 2-D DWT for two-level decomposition, b 2-D SSRWT for two-level decomposition

$$CR_{(X,Y)} = \frac{\sum_{j=1}^{k} (X_j - \mu_X)(Y_j - \mu_Y)}{k - 1}.$$
 (3)

(a)

In PCA transformation, data are translated and rotated to adapt the new axes representing the principal components, calculated by Eq. 4 using linear transformation. Here, $E_{\rm vec}$ and $E_{\rm vec}^T$ denote eigenvectors and transpose of eigenvectors, respectively. C_oR represents correlation matrix through which $E_{\rm vec}$ and $E_{\rm vec}^T$ are computed.

$$V = E_{\text{vec}} C_o R E_{\text{vec}}^T \tag{4}$$

The coefficients present in column of eigenvector matrix E_{vec} which need to transform the original image values into principal component values using Eq. 5, where P denotes the number of principal components, pc represents the principal component value calculated with respect to band i, and l representing total number of input bands with pixel value px (Pohl & Van Genderen, 2016; Vivone et al., 2015).

(b)

$$P_{pc} = \sum_{i=1}^{l} p x_i E_{\text{vec}}^{(i,px)} \tag{5}$$

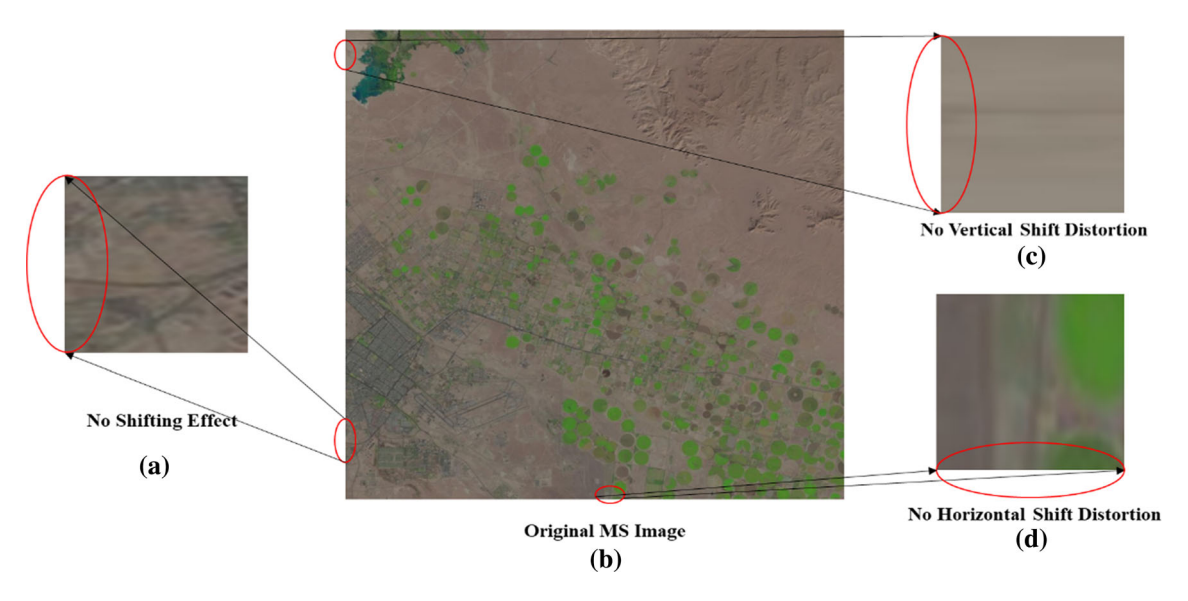


Fig. 4 Original MS image (data set 1) with a No shifting effect, b Original MS image, c No vertical shift distortion, d No horizontal shift distortion

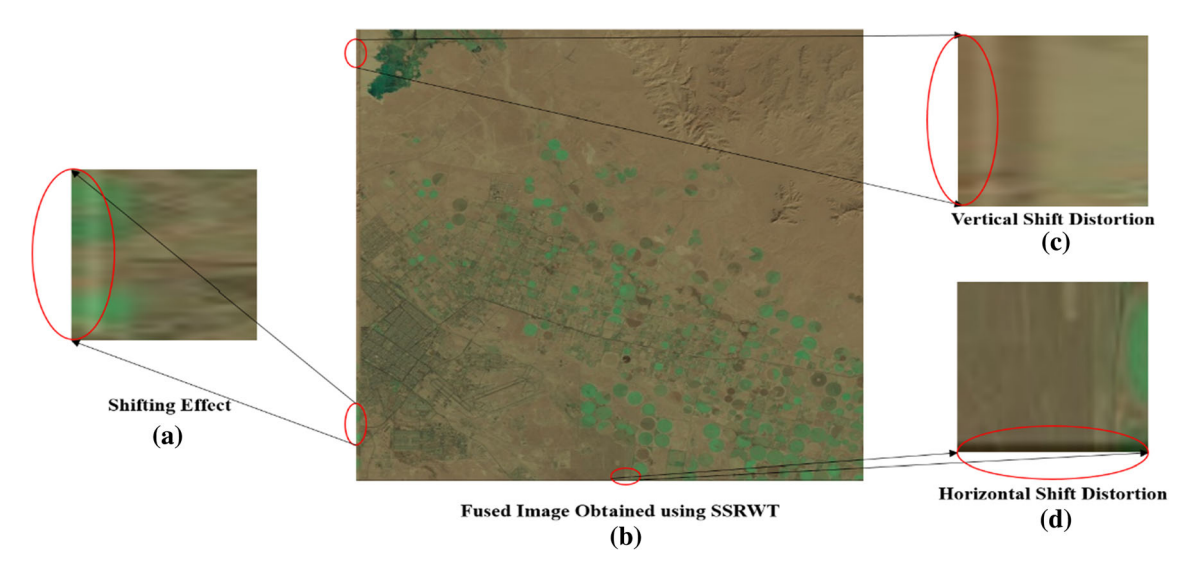


Fig. 5 Fused image (data set 1) of SSRWT with a shifting effect, b fused image obtained using SSRWT, c vertical shift distortion, d horizontal shift distortion

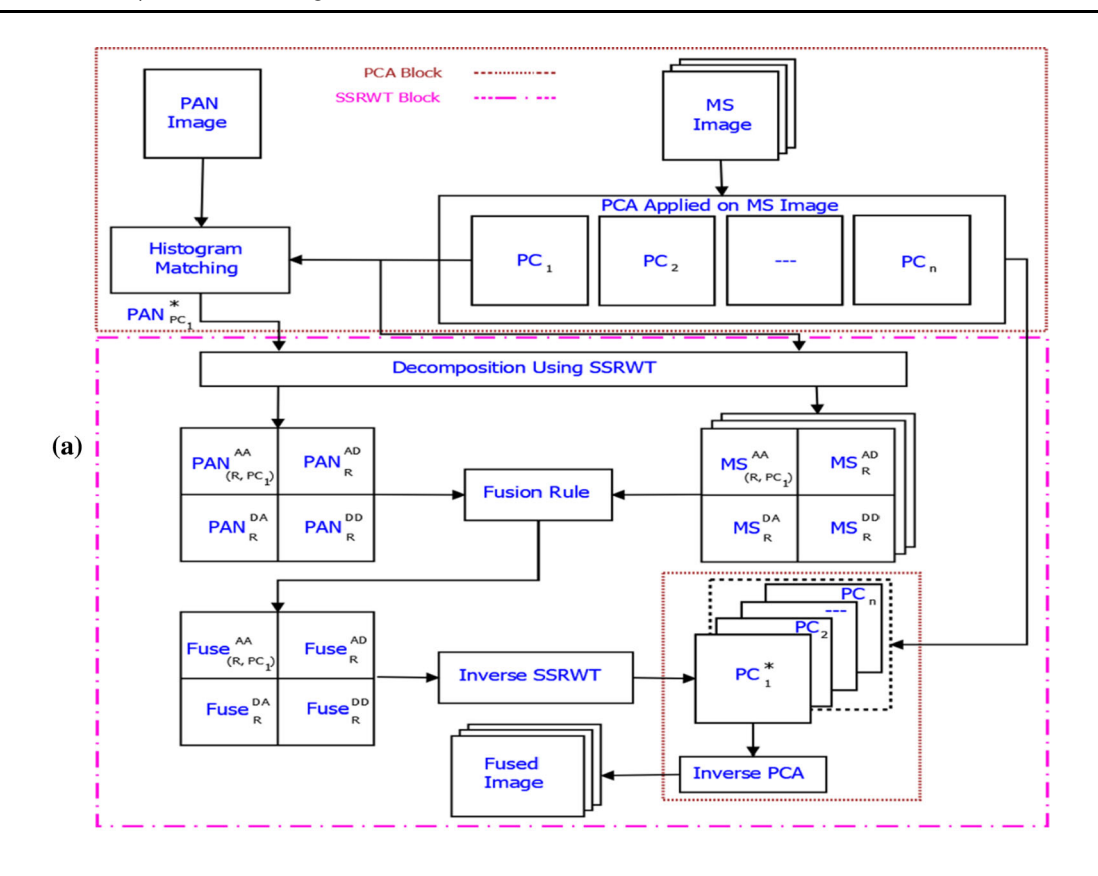
Applying the inverse PCA transform, the combined data can be transformed back to the original co-ordinate system. In general, spatial information is present in the first principal component, PC_1 , which is present in all bands while spectral information which is specific to individual bands and is present in remaining principal components $(PC_2, ..., PC_n)$. PC_1 is replaced by PAN^* which is histogram matched with original PAN image. Then, inverse PCA is performed to obtain resultant fused image. This fused image is spatially high but spectrally degraded.

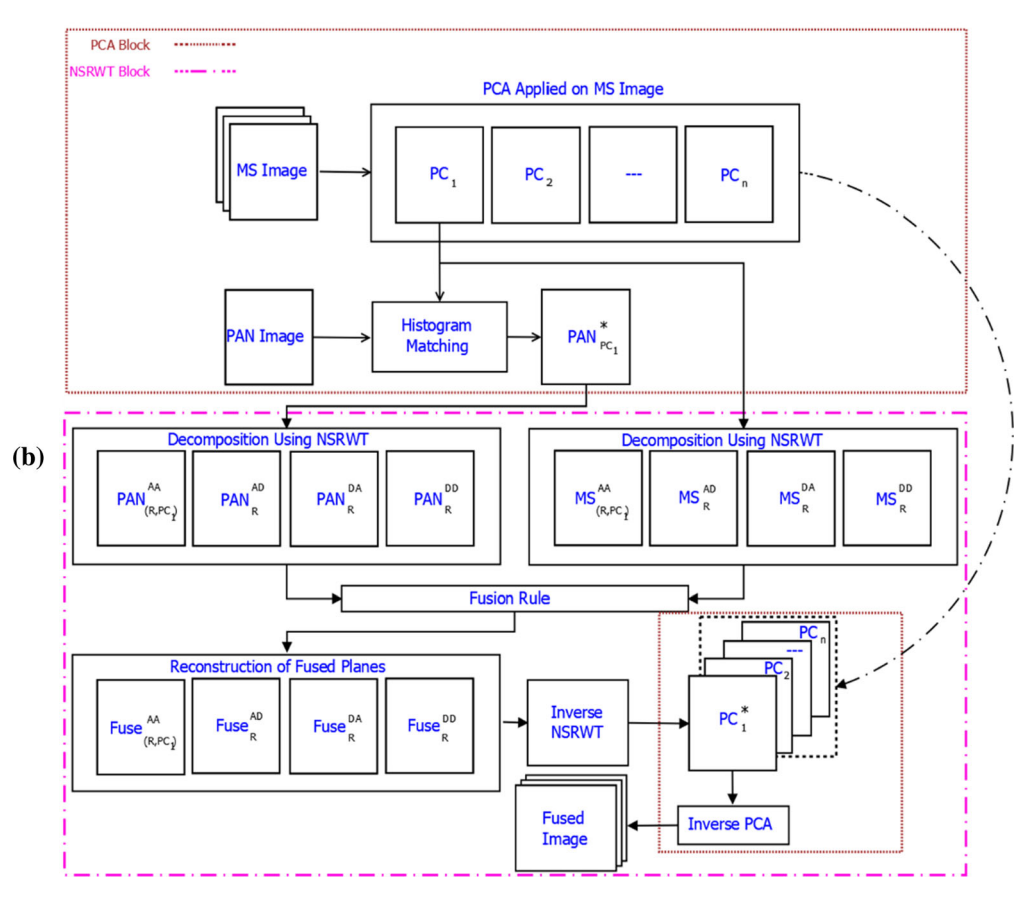
Fig. 6 Block schematic a PCA-SSRWT fusion algorithm, b PCA-▶NSRWT fusion algorithm

Subsampled Rotated Wavelet Transform (SSRWT)

SSRWT is modified interpretation of 2D DWT. Standard 2D DWT gives edge information in three directions (0°, 90° and $\pm 45^{\circ}$). Out of these orientations, combined diagonal edge information can be separated and presented in two orientations as $+45^{\circ}$ and -45° using SSRWT. In 2D









DWT, decomposition is performed using 1D DWT filter coefficients, while SSRWT uses nonseparable 2D rotated wavelet filters. These 2D rotated wavelet filters are designed using product of 1D scaling and wavelet functions given by Eqs. 6–9.

$$H^{AA} = \phi^{AA}(x, y) = \phi(x)\phi(y) \tag{6}$$

$$H^{AD} = \psi^{AD}(x, y) = \phi(x)\psi(y) \tag{7}$$

$$H^{DA} = \psi^{DA}(x, y) = \psi(x)\phi(y) \tag{8}$$

$$H^{DD} = \psi^{DD}(x, y) = \psi(x)\psi(y).$$
 (9)

1D scaling and wavelet functions are used to generate 2D filters H^{AA} , H^{AD} , H^{DA} and H^{DD} . These 2D filter masks are then rotated by $+45^{\circ}$ or -45° to design new filter masks $H^{AA}_{R(\theta)}$, $H^{AD}_{R(\theta)}$, $H^{DA}_{R(\theta)}$ and $H^{DD}_{R(\theta)}$ which are referred as

rotated wavelet filters (RWF) (Kim & Udpa, 2000). Here, subscript R is the fact that filters are rotated by $\theta = +45^{\circ}$ or -45° while superscript AA (approximation), AD (horizontal), DA (vertical) and DD (diagonal) are four subband images. Two levels of decomposition for image F(x,y) with size $m \times n$ using 2D SSRWT are shown in Fig. 2. After first level of decomposition, four subband images I^{AA} , I^{AD} , I^{DA} and I^{DD} are generated of size $\frac{m}{2} \times \frac{n}{2}$ using 2D RWF.

To obtain finer resolution in low frequency band, subband image I^{AA} can be further decomposed to generate subband images \hat{I}^{AA} , \hat{I}^{AD} , \hat{I}^{DA} and \hat{I}^{DD} of size $\frac{m}{4} \times \frac{n}{4}$ as shown in Fig. 2. Applying 2D RWF on image F(x,y), we can extract information in $+45^{\circ}$ and -45° distinctly. The Fourier spectrum for 2D DWT provides information in

econd Level

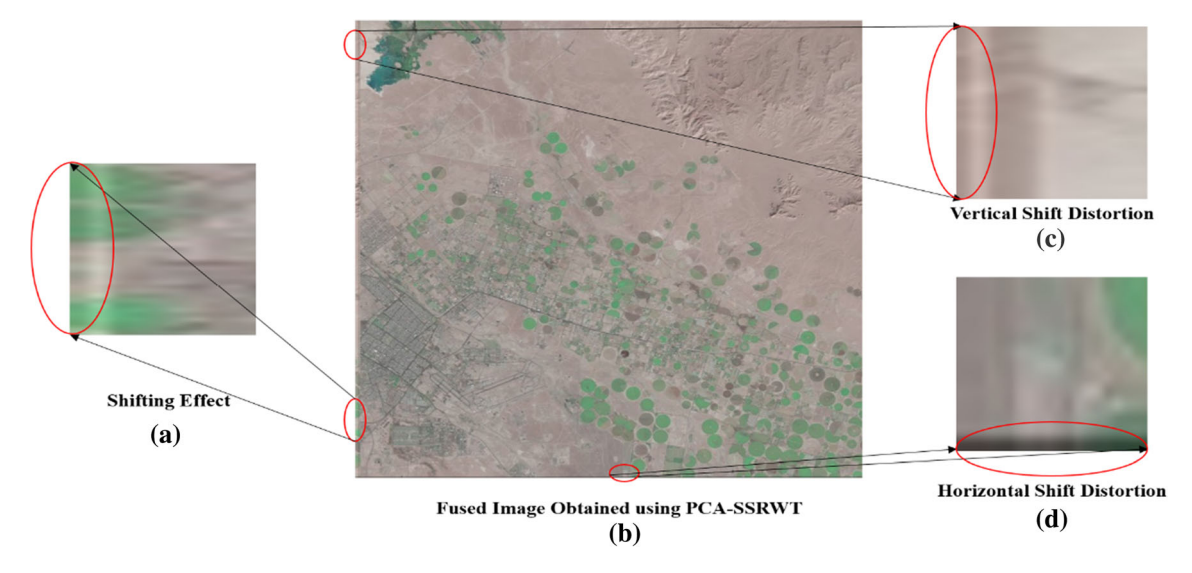


Fig. 7 Fused image (data set 1) of PCA-SSRWT with **a** shifting effect, **b** fused image obtained using PCA-SSRWT, **c** vertical shift distortion, **d** horizontal shift distortion

H_{R(**O**)}

H_{R(**O**)}

m×r

I_{m×n}



Fig. 8 Two-level decomposition

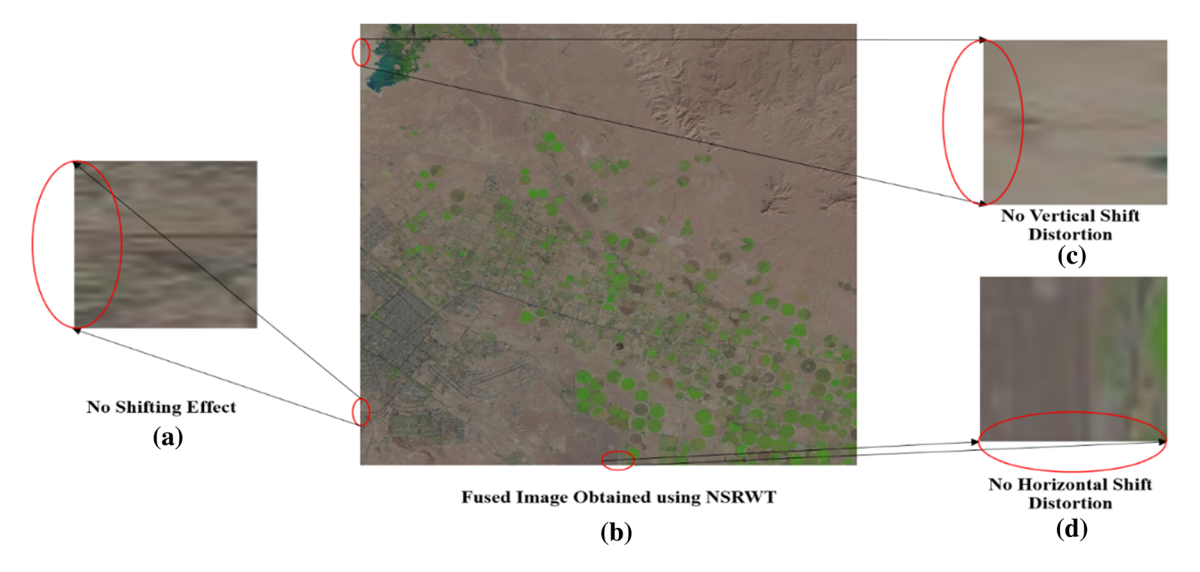


Fig. 9 Fused image (data set 1) of NSRWT with a no shifting effect, b fused image obtained using NSRWT, c no vertical shift distortion, d no horizontal shift distortion

three direction is shown in Fig. 3a where as SSRWT provides information in 0° , 90° , $+45^{\circ}$ and -45° as shown in Fig. 3b.

SSRWT decomposition is applied to generate four subband images for each, MS and PAN images. Using fusion rule, corresponding four subband images are merged. It is followed by inverse SSRWT to get the final fused image. Figure 4 shows original MS image (Fig. 4b) with no visual artifacts (Fig. 4a, c, d). The fused image obtained by SSRWT (Fig. 5b) shows three major visual artifacts namely color distortion, shifting effect (Fig. 5a) and shift distortion along vertical columns and horizontal rows as shown in Fig. 5c, d, respectively.

Color distortion observed in fused image of SSRWT is caused as standard deviation of green (g) band of input MS image is higher than red (r) and blue (b) bands, and the resultant fused image tends to be greenish.

Proposed Fusion Algorithms

Standard PCA Integrated with Subsampled Rotated Wavelet Transform (PCA-SSRWT)

To overcome color distortion, a hybrid satellite image fusion algorithms are used which integrate PCA with SSRWT (PCA-SSRWT). Figure 6a illustrates the block

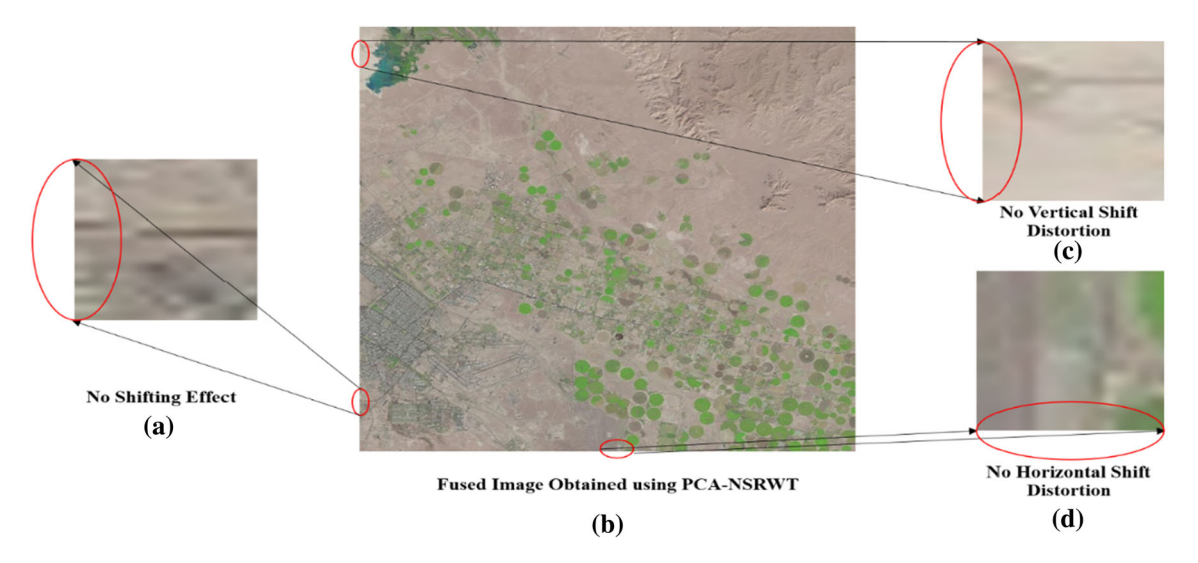


Fig. 10 Fused image (data set 1) of PCA-NSRWT with a no shifting effect, b fused image obtained using PCA-NSRWT, c no vertical shift distortion, d no horizontal shift distortion



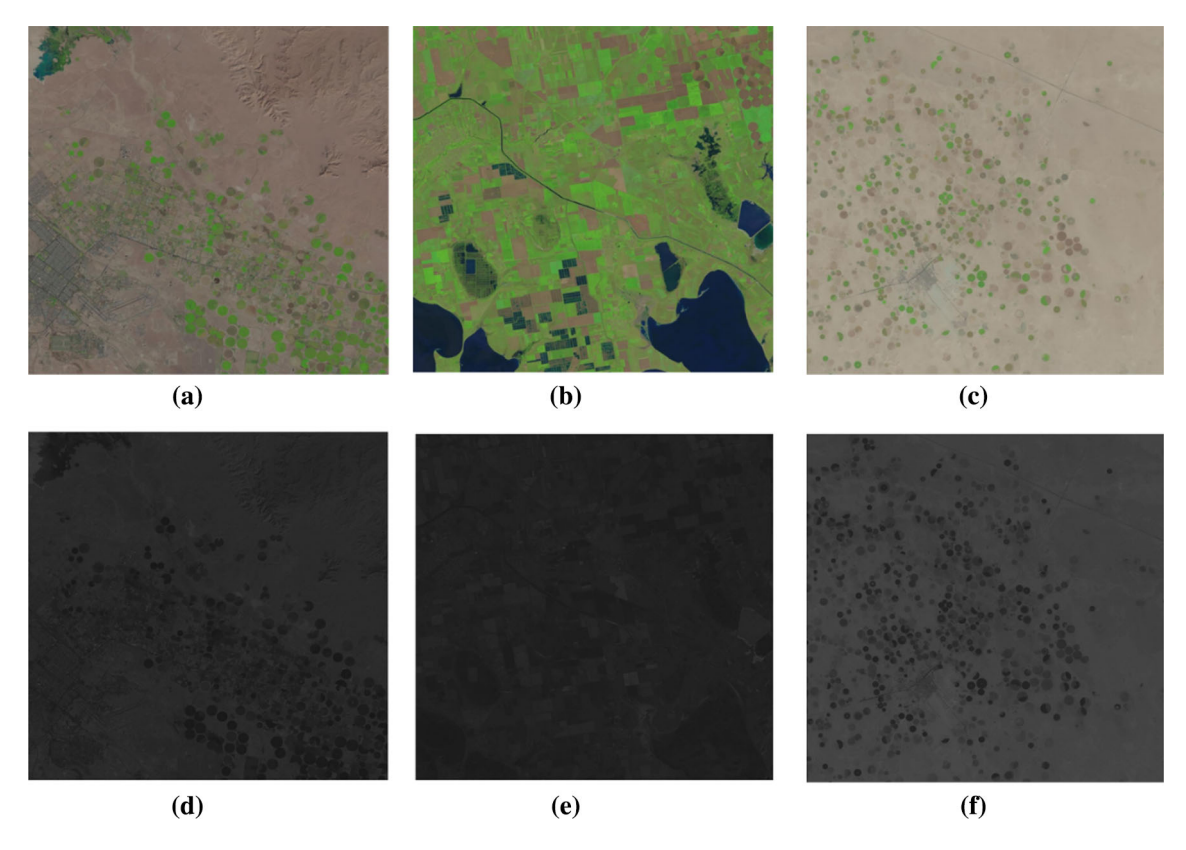


Fig. 11 LANDSAT-8 OLI sensor data sets a MS image (data set 1), b PAN image (data set 1), c MS image (data set 2), d PAN image (data set 2), e MS image (data set 3), f PAN image (data set 3)

schematic of PCA–SSRWT. The brown and magenta color dotted lines represent PCA and SSRWT blocks, respectively. PCA transformation is applied on MS bands to get the principal components $(PC_1, ..., PC_n)$. The first principal component PC_1 has maximum spatial characteristics which are common in all individual bands of MS image. Remaining principal components carry spectral information specific to individual r, g, and b bands of MS image. Then, PAN image and PC_1 of MS band are histogram matched to generate $PAN_{PC_1}^*$.

SSRWT decomposition is applied on PC_1 and $PAN_{PC_1}^*$, which in turn generates four subband images each as shown in Fig. 6a. After applying SSRWT to extract features on $PAN_{PC_1}^*$, it generates four subband images $PAN_{(R,PC_1)}^{AA}$, PAN_R^{AD} , PAN_R^{DA} and PAN_R^{DD} representing approximation, horizontal, vertical and diagonal subbands, respectively. Similarly, SSRWT decomposition of PC_1 generates four subband images $PAN_{(R,PC_1)}^{AD}$, PAN_R^{AD} , PAN_R^{DA} , PAN_R

Four composite subband images, $FUSE_{(R,PC_1)}^{AA}$, $FUSE_R^{AD}$, $FUSE_R^{DD}$ corresponding to approximation, horizontal, vertical and diagonal details are, respectively,

created using fusion rules. Inverse SSRWT is applied to reconstruct spatially high image PC₁*. This component along with remaining principal components (PC₂,...,PC_n) are used together for inverse PCA transform to get resultant fused image. The fused image (Fig. 7b) generated is spatially high by taking advantage of PCA for spatial details in which color distortion has been mitigated as shown in Fig. 7 using PCA–SSRWT. The final fused image obtained using PCA–SSRWT is spectrally low and carries visual artifacts namely shifting effect (Fig. 7a) and shift distortion (Fig. 7c, d) due to down sampling and upsampling process of SSRWT. To overcome these visual artifacts and at the same time to maintain spatial quality and improve spectral quality of the fused image, NSRWT is preferred over SSRWT.

Standard PCA Integrated with Nonsubsampled Rotated Wavelet Transform (PCA-NSRWT)

The visual artifact, i.e., shifting effect which is caused during down-sampling while shift distortion is caused during up-sampling is observed in the fused image obtained by SSRWT and PCA-SSRWT. To overcome these two visual artifacts, NSRWT is used which is



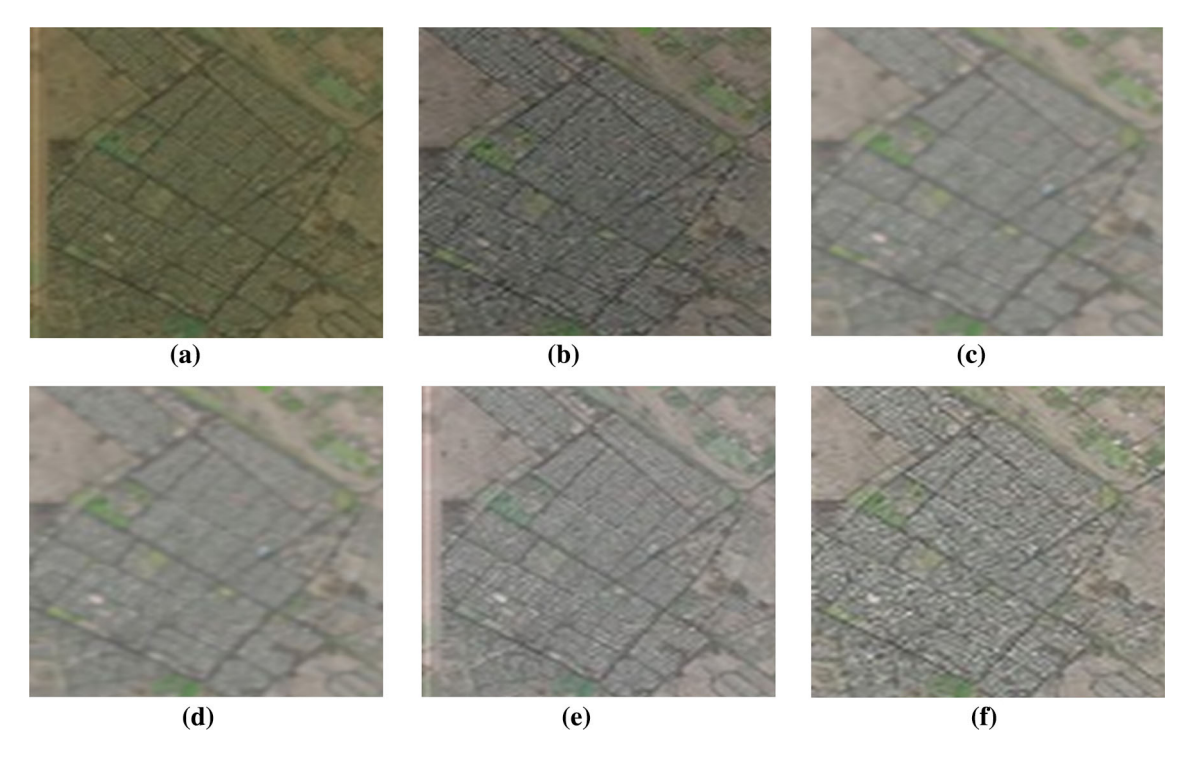
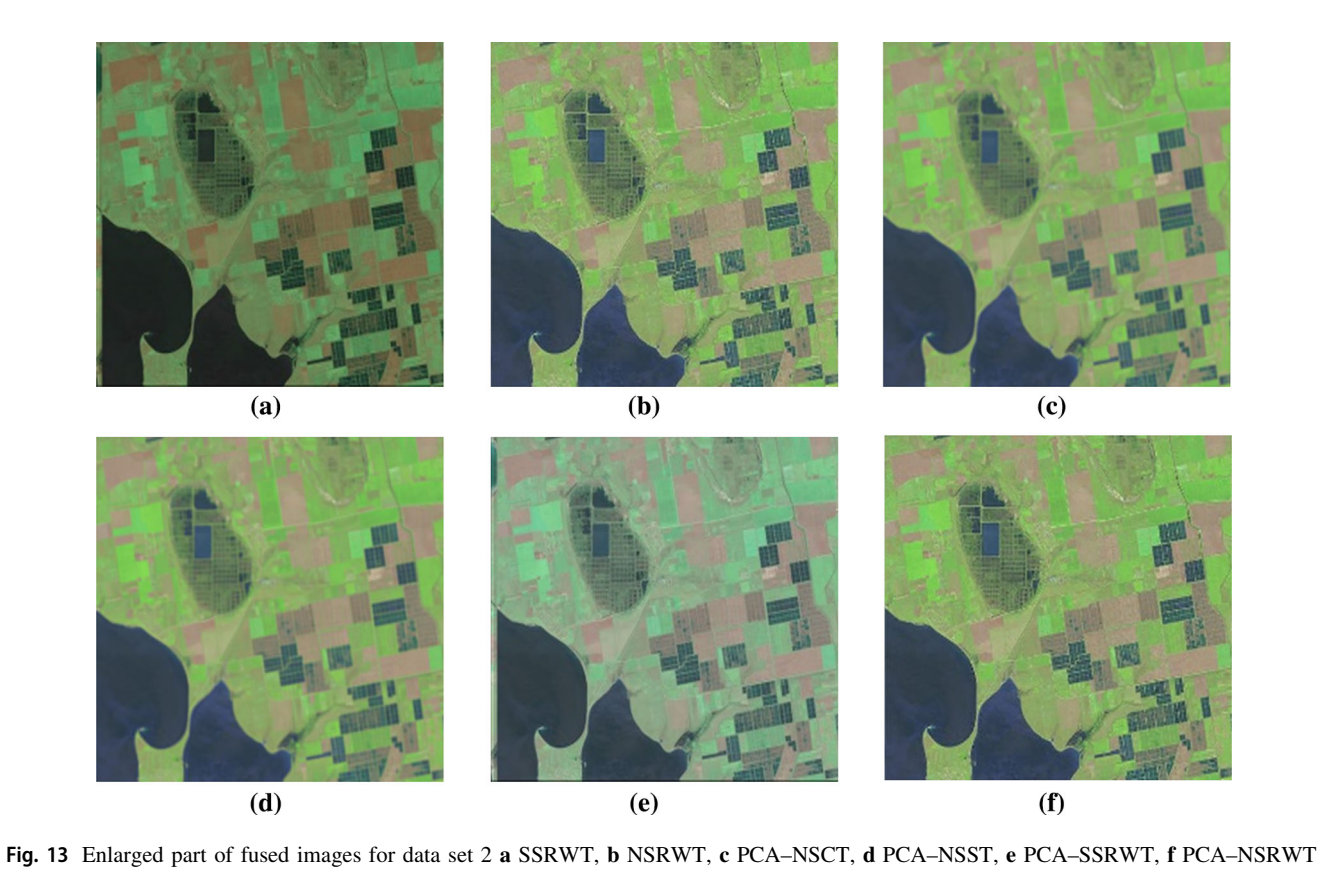


Fig. 12 Enlarged part of fused images for data set 1 a SSRWT, b NSRWT, c PCA-NSCT, d PCA-NSST, e PCA-SSRWT, f PCA-NSRWT



undecimated version of SSRWT (Chavan et al., 2018). The two-level decomposition of an image F(x, y) with size $m \times m$ working of NSRWT is same as that of SSRWT except the



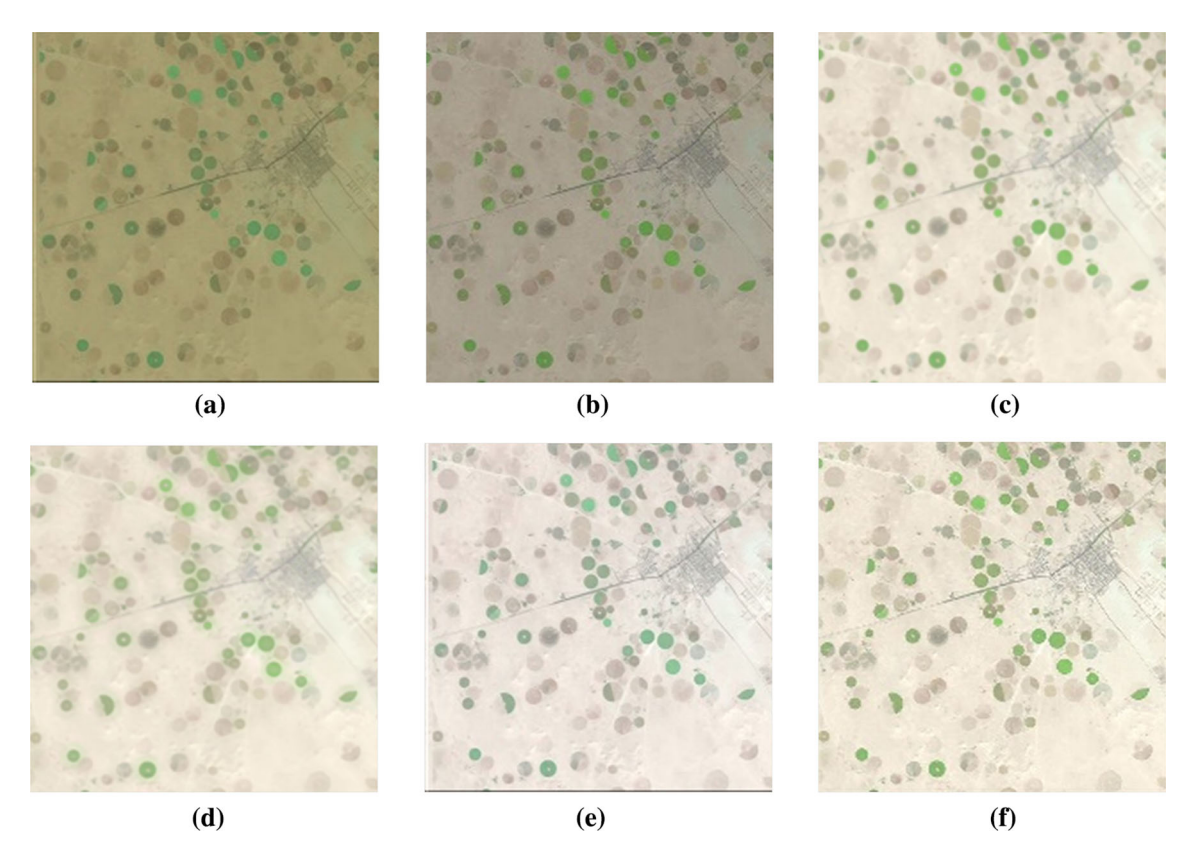


Fig. 14 Enlarged part of fused images for data set 3 a SSRWT, b NSRWT, c PCA-NSCT, d PCA-NSST, e PCA-SSRWT, f PCA-NSRWT

fact that we do not perform subsampling in the process. Therefore, the size of subband images after decomposition remains same as that of input images. As we are eliminating the process of sub-sampling, visual artifacts which were observed in SSRWT are not observed in fused image obtained using NSRWT. The final fused image obtained is shown in Fig. 9b, where no visual artifacts (Fig. 9a, c, d) are observed, but spatially it is degraded with improved spectral quality. Therefore, to improve the spatial quality of the fused image, PCA is integrated with NSRWT (PCA–NSRWT).

The working principle of PCA–NSRWT is similar to that of PCA–SSRWT except the sub-sampling is eliminated in PCA–NSRWT. Figure 6b shows the block schematic of PCA–NSRWT. The brown dotted and magenta dotted lines represent PCA and NSRWT blocks, respectively. As shown in Fig. 6b, PCA is applied on the input MS generating PC₁ which is then histogram matched with PAN image to generate new histogram matched image, PAN $_{PC_1}^*$. Now, NSRWT decomposition is applied on PC₁ and PAN $_{PC_1}^*$ to generate four subband images for each PC₁ (MS $_{(R,PC_1)}^{AA}$, MS $_R^{AD}$, MS $_R^{DA}$ and MS $_R^{DD}$) and PAN $_{PC_1}^*$ (PAN $_{(R,PC_1)}^{AA}$, PAN $_R^{DA}$ and PAN $_R^{DD}$). Then using fusion rule, four composite subband planes FUSE $_{(R,PC_1)}^{AA}$, four composite subband planes FUSE $_{(R,PC_1)}^{AA}$,

FUSE_R^{AD}, FUSE_R^{DA} and FUSE_R^{DD} are generated on which inverse NSRWT is applied to get PC₁*.

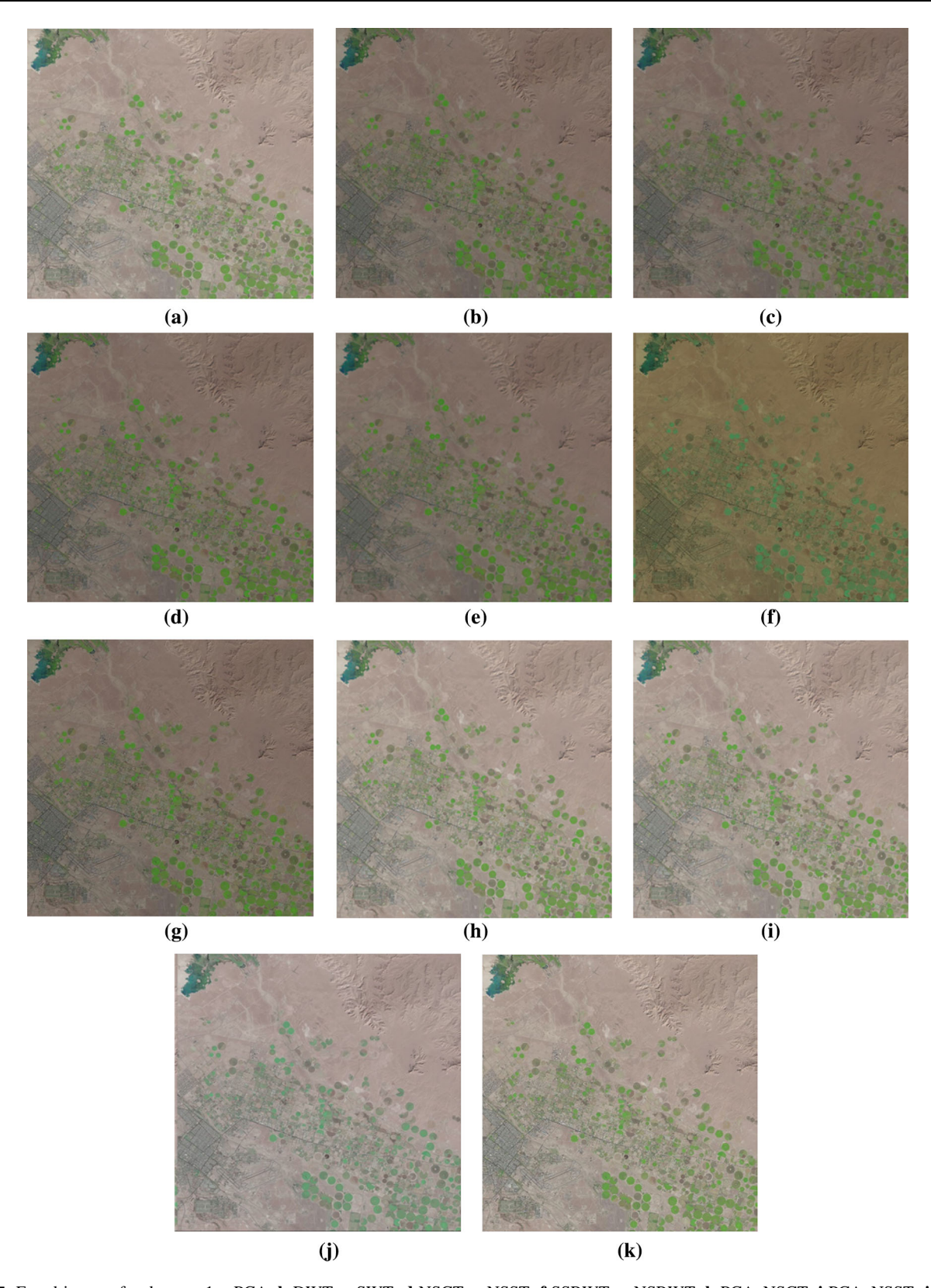
This newly generated image PC₁* which is spatially high is combined with remaining principal components of MS, which are spectrally high. Later, inverse PCA is applied to generate final fused image. The final fused image obtained from PCA–NSRWT is spectrally as well as spatially high with no visual artifacts and no color distortion which was observed in SSRWT and NSRWT. Figure 10b shows fused image obtained using PCA–NSRWT with enhanced spectral quality, and no visual artifacts (Fig. 10a, c, d).

Result and Discussion

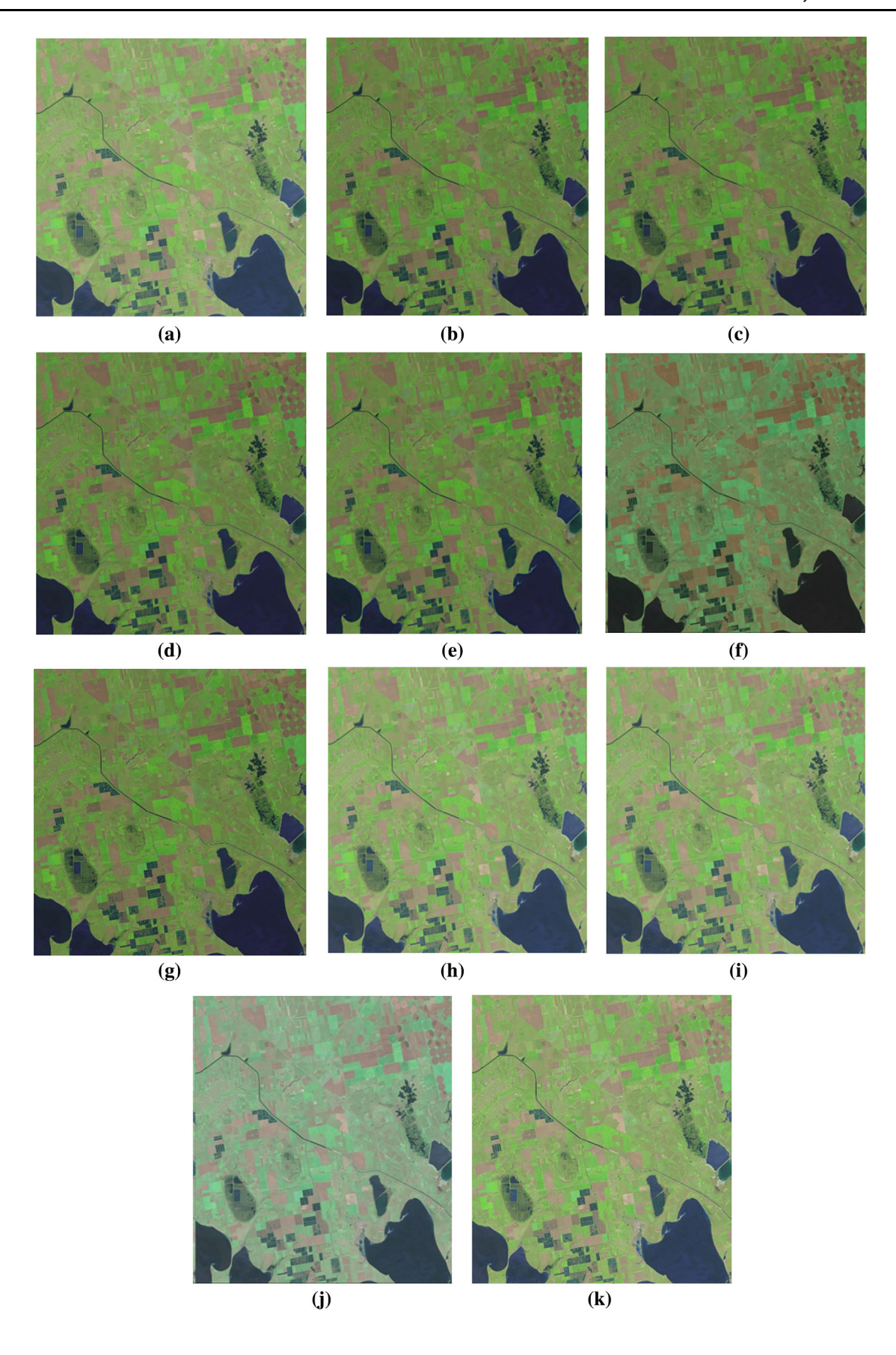
Data Sets

Experimentation was carried out on MS and PAN images recorded by LANDSAT-8 OLI sensor. LANDSAT-8 OLI sensors have nine bands out of which band 2, 3 and 4 are considered for multispectral images captured through 0.45–0.51 m μ , 0.53–0.59 m μ , and 0.63–0.67 m μ bandwidth range representing r, g, and b bands, respectively. PAN band is recorded through 0.50–0.68 m μ bandwidth range. MS and PAN images have 30 and 15 m resolution, respectively. Both MS and PAN images are co-registered





 $\textbf{Fig. 15} \ \ \text{Fused images for data set 1 a PCA, b DWT, c SWT, d NSCT, e NSST, f SSRWT, g NSRWT, h PCA-NSCT, i PCA-NSST, j PCA-SSRWT, k PCA-NSRWT \\$





▼Fig. 16 Fused images for data set 2 a PCA, b DWT, c SWT, d NSCT, e NSST, f SSRWT, g NSRWT, h PCA-NSCT, i PCA-NSST, j PCA-SSRWT, k PCA-NSRWT

with each other. Figure 11 shows three pairs of MS and PAN images with first row representing MS images (Fig. 11a, c, e) and second row PAN images (Fig. 11b, d, f). Performance evaluation of the fused image is carried out using visual interpretation and quantitative analysis.

Visual Interpretation

For visual interpretation and quantitative analysis, proposed satellite fusion algorithms, i.e., PCA–SSRWT and PCA–NSRWT are compared with PCA, DWT, SWT, NSCT, NSST, SSRWT, NSRWT, PCA–NSCT and PCA–NSST. The fused images for proposed algorithms along with various state-of-the-art pansharpening methods are shown through Figs. 15a–k, 16a–k and 17a–k for three data sets, respectively. Further, we have compared the proposed method with the pan-sharpening algorithms incorporated in commercial software such as ArcGIS and ERDAS imagine.

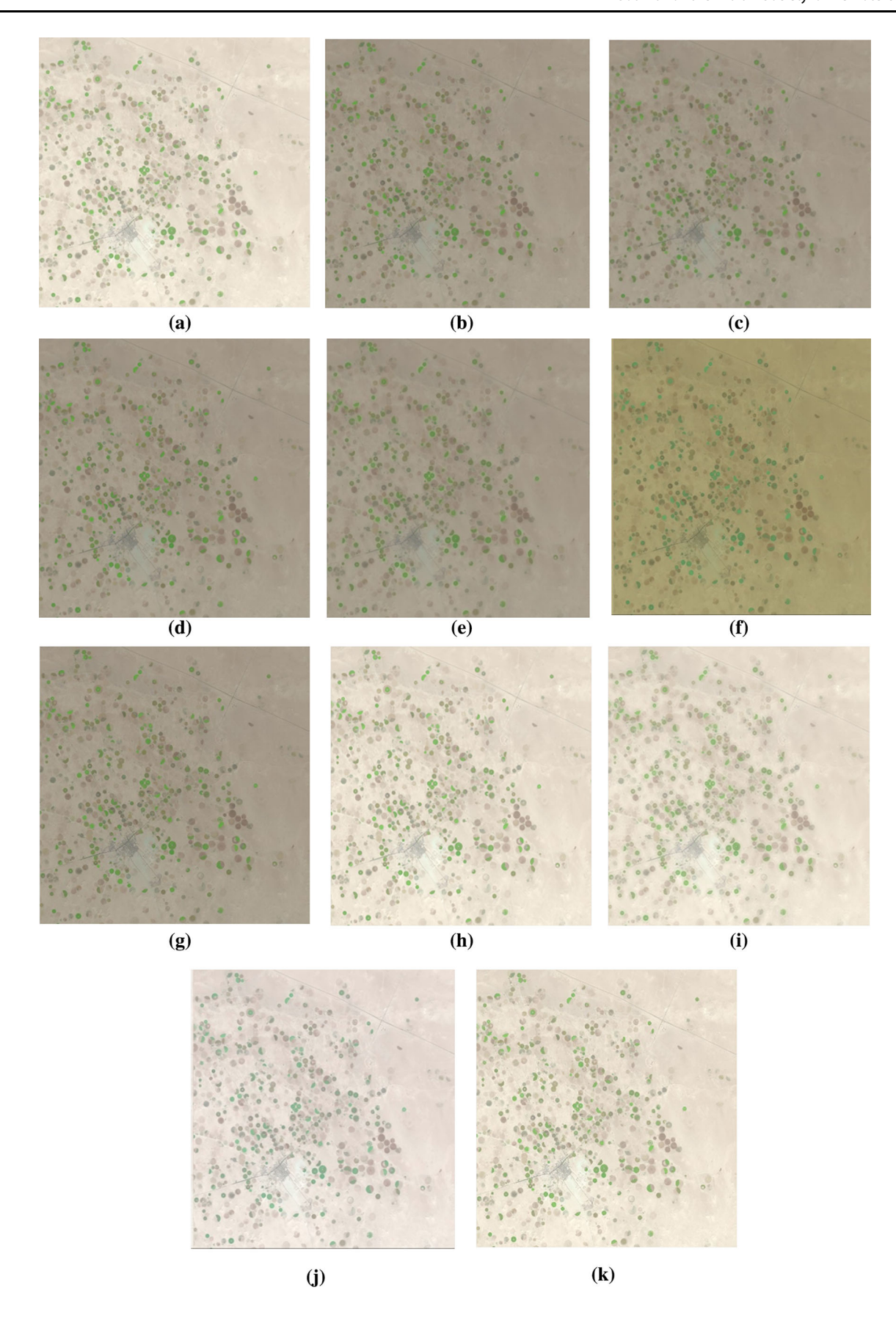
Figures 12a-f, 13a-f and 14a-f show enlarged part of fused images obtained using SSRWT, NSRWT, PCA-NSCT, PCA-NSST, PCA-SSRWT and PCA-NSRWT for three data sets. Significant color distortion is visible in the fused images obtained using SSRWT (Figs. 12a, 13a, 14a) as standard deviation of g band is more than r and b bands. The fused images as a result of SSRWT not only suffer from color distortion but also introduce visual artifacts like shifting effect and shift distortion caused due to process of subsampling. The fused images obtained using NSRWT (Figs. 12b, 13b, 14b) do not show color distortion, and shifting effect and shift distortion are also not observed. Figures 12e, 13e and 14e show the fused images obtained using PCA-SSRWT. When Fig. 13a is compared with Fig. 13e, the color of water bodies (bottom left corner or bottom right corner) is much better in the latter image. In Fig. 13a, water bodies appear to be completely black body, whereas in Fig. 13e it appears to be blue which suggests that color distortion is less in fused images obtained using proposed PCA-SSRWT than SSRWT. Though spectral and spatial quality of fused image is improved using PCA-SSRWT, it suffers from shifting effect and shift distortion as clearly seen in Figs. 12e, 13e and 14e on left vertical columns and bottom horizontal rows. Enlarged part of the fused images obtained using PCA-NSCT and PCA-NSST is shown through Figs. 12c, d, 13c, d and 14c, d, respectively. It is evident that the fused images do not suffer from spectral distortion and resemble closely to original input images. Though spectrally high but the fused images obtained using PCA-NSCT, PCA-NSST suffer from blurring effect (Fig. 12c, d), boundary of water bodies (Fig. 13c, d) and farms (Fig. 14c, d) are not sharp enough to be discriminated. However, visually the fused images obtained using PCA–NSCT and PCA–NSST appear to be similar.

The fused image as a result of PCA-NSRWT has sharp edges around the water bodies (Fig. 13f) and does not show color distortion. It is closely resembling to the input images which shows that the fused image is of high spectral quality. In Figs. 12f and 14f, one can clearly discriminate objects, i.e., residential areas with road intersections in Fig. 12f and cultivated/harvested farms in Fig. 14f. However, it is difficult to interpret visually using NSRWT (Figs. 12f, 14f).

Among pansharpening algorithms used for comparison, the fused images using PCA (Figs. 15a, 16a, 17a) are spatially high which make them visually appealing and attractive. However, they suffer with color distortion considerably which suggest that they are spectrally distorted. The fused images using DWT (Figs. 15b, 16b, 17b) and SWT (Figs. 15c, 16c, 17c) show no color distortion but blurring effect. The boundaries of farms in Figs. 16b, c and 17b, c are difficult to discriminate each farm. The edges of water bodies (Fig. 16b, c) do not appear to be sharp enough which shows that spatial quality of fused images as result of DWT and SWT is poor. Figures 15d, 16d and 17d and Figs. 15e, 16e and 17e show the fused images obtained using NSCT and NSST, respectively. Figures 15d, 16d and 17d clearly show that the NSCT does not suffer from color distortion and incorporates almost all spectral information from MS and PAN images. It is difficult to distinguish small details in the fused images which indicated that NSCT fails to incorporate spatial details. However, NSCT appears better than DWT and SWT and resembles closely to source images. Figure 15e, 16e and 17e show the fused image obtained using NSST with no color distortion and improved spatial quality. However, it is clear from Fig. 16d, e that NSCT captures edges of water bodies where NSST fails. Figure 18 presents the fused images obtained from the pan-sharpening algorithms incorporated into ArcGIS and ERDAS imagine software. The first row in Fig. 18a, considerable spectral distortion (color of water bodies), is observed in fused image obtained by GS, IHS and Brovey. The second row in Fig. 18b shows the fused image generated using Hyper-spherical Color Sharpening (HCS), high-pass filtering (HPF) and Ehlers algorithms (incorporated in ERDAS Imagine). It is obvious that the fused images are spatially low and suffer from blurring effect.

The fused image as a result of PCA-NSRWT is not only visually superior to that of individual PCA, SSRWT, NSRWT, NSCT, NSST, PCA-NSCT, PCA-NSST and PCA-SSRWT but also has enhanced spectral and spatial







▼Fig. 17 Fused images for data set 3 a PCA, b DWT, c SWT, d NSCT, e NSST, f SSRWT, g NSRWT, h PCA-NSCT, i PCA-NSST, j PCA-SSRWT, k PCA-NSRWT

quality of the fused image without introducing any visual artifacts. It has almost retained all color information corresponding to original input MS images.

Quantitative Analysis

The quantitative analysis for the proposed algorithms along with various state-of-the-art methods is presented in Tables 1, 2 and 3 for three pairs of MS and PAN images. In both Tables, the best results are represented black bold font and the second best results are marked with underline values. Ideal values for all the performance metrics are presented by reference value in second row of both the tables. Table 1 reports the experimental results for conventional fusion metrics which includes correlation coefficient (CC), entropy (H), structural similarity index metric (SSIM) and spatial frequency (SF) (Jagalingam & Hegde, 2015). To observe the error rate of fused image, mean square error (MSE) (Jagalingam & Hegde, 2015) is used. In addition, Table 2 presents the spectral angle mapper (SAM), universal image quality index (UIQI) and quality

not requiring reference (QNR) are used as assessment metrics for spectral quality of the fused images (Palsson et al., 2016).

SSIM measures the structural similarity through local patterns of pixel between fused and original images. It uses standard deviation and means of fused and original images. SSIM ranges from -1 to +1, and values near to +1indicate that fused and original images are similar. Another way to observe the similarity between fused and input images is to compute row and column frequency of fused image. Higher the value of SF, more is the similarity between input and fused images. Spectral distortion in fused image is measured using MSE. SAM denotes spectral angle between original and estimated spectral vectors (Palsson et al., 2016). If value of SAM is equal to zero, then spectral distortion is absent otherwise spectral distortion is present. Usually, SAM is measured either in degrees or radians. UIQI is used widely for assessing quality of the fused images (Palsson et al., 2016). It maps distortion by combining three factors which includes loss of correlation, luminance distortion and contrast distortion. The best value of UIOI is + 1. ONR is used as average assessment metric which combined spectral distortion (D_{λ}) and spatial distortion $(D_{\rm MS})$ (Palsson et al., 2016). When QNR is 1, values of D_{λ} and D_{MS} are zero, i.e., no spectral and spatial distortion observed in the fused image. The

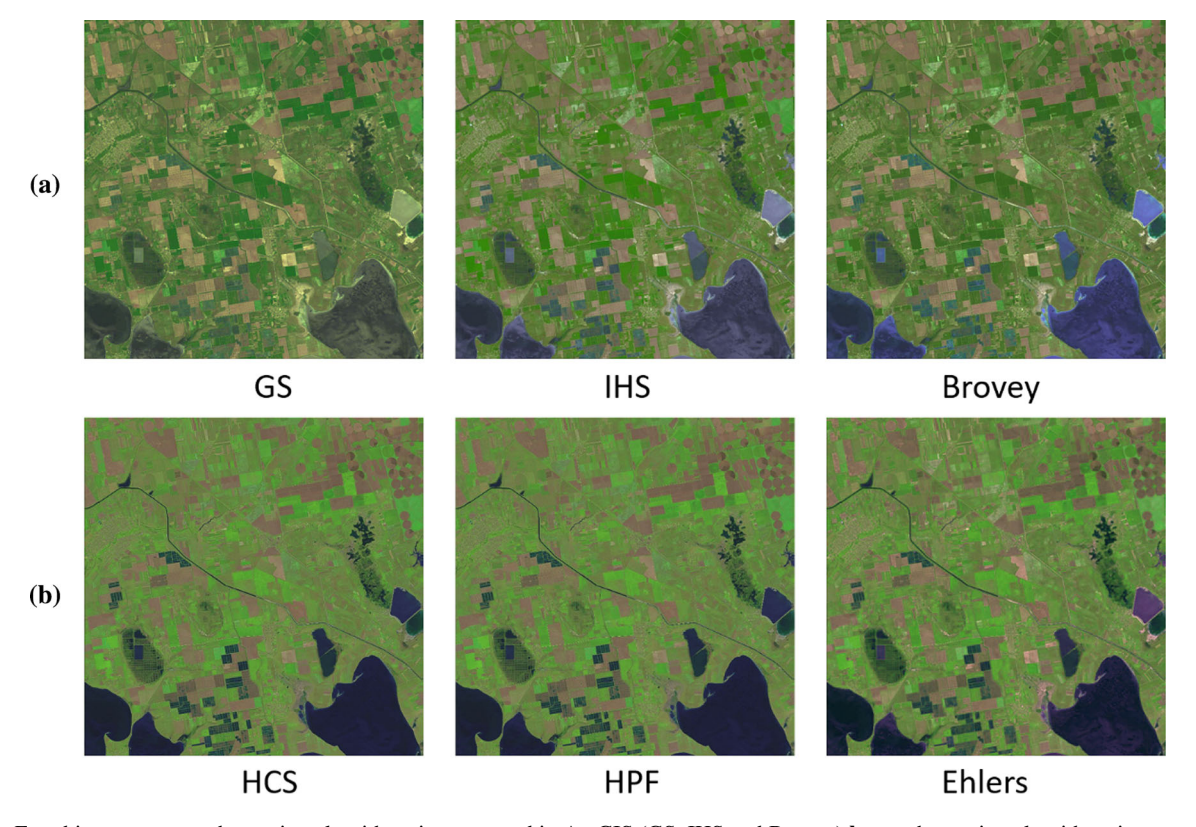


Fig. 18 Fused images: a pan-sharpening algorithms incorporated in ArcGIS (GS, IHS and Brovey) b pan-sharpening algorithms incorporated in ERDAS Imagine (HCS, HPF and Ehlers)



Table 1 Quantitative analysis of the fused images based on statistical metrics

Dataset	Methods/parameters	CC	Н	SSIM	SF	MSE
Dataset 1	PCA	0.8336	6.25	0.9158	3.22	1770.98
	DWT	0.8337	5.96	0.9061	2.32	1803.54
	SWT	0.8333	5.96	0.9301	2.28	1804.11
	NSCT	0.8411	5.96	0.9331	2.10	1803.33
	NSST	0.8467	5.91	0.9059	2.87	69.5639
	SSRWT	0.4858	6.12	0.6780	2.32	2642.44
	NSRWT	0.8171	6.07	0.8962	4.02	1695.56
	PCA-NSCT	0.8409	6.21	0.8879	4.11	71.1007
	PCA-NSST	0.9674	6.31	0.9855	4.01	78.8710
	PCA-SSRWT	0.4884	6.11	0.7336	3.27	298.317
	PCA-NSRWT	0.9709	6.39	0.9917	5.72	67.8014
Dataset 2	PCA	0.6903	6.91	0.9270	2.54	1338.25
	DWT	0.6362	6.83	0.9296	2.19	1286.97
	SWT	0.6358	6.83	0.9453	2.20	1288.01
	NSCT	0.6391	6.83	0.9455	2.02	1287.98
	NSST	0.8901	6.82	0.9388	2.79	46.0483
	SSRWT	0.3634	6.72	0.7811	2.29	1448.51
	NSRWT	0.6233	6.89	0.9327	3.56	1212.22
	PCA-NSCT	0.6917	6.90	0.9722	3.37	113.992
	PCA-NSST	0.9860	6.89	0.9929	3.12	259.665
	PCA-SSRWT	0.3878	6.46	0.6723	2.65	589.307
	PCA-NSRWT	0.9890	6.97	0.9970	4.44	37.6471
Dataset 3	PCA	0.9629	6.21	0.9283	2.29	4314.81
	DWT	0.9463	5.80	0.8786	1.45	4331.92
	SWT	0.9462	5.80	0.9276	1.41	4332.89
	NSCT	0.9498	5.80	0.9292	1.38	4331.74
	NSST	0.9617	5.76	0.9144	2.20	65.9204
	SSRWT	0.5843	5.97	0.6957	1.62	5846.87
	NSRWT	0.9361	5.86	0.9218	2.44	4054.95
	PCA-NSCT	0.9633	6.20	0.9560	3.22	93.0862
	PCA-NSST	0.9574	6.15	0.9854	2.66	312.312
	PCA-SSRWT	0.5083	6.04	0.8267	2.42	360.455
	PCA-NSRWT	0.9722	6.28	0.9977	3.95	36.2700

lowest value of QNR is zero with increase in D_{λ} and D_{MS} values.

As reported in Table 1, PCA–NSRWT outperforms traditional pansharpening methods based on entropy and spatial frequency. The fused image obtained by PCA–NSRWT has richer information than any other methods. Fused image of PCA–NSRWT has incorporated most of the information from input MS and PAN images. SSRWT and PCA–SSRWT perform poorly as compared to the proposed method as it suffers from shift distortion and shifting effect. The fused image obtained by PCA–NSCT (dataset 1 and 2) performs better than other methods and are highly correlated with input MS and PAN images. For dataset 3, PCA–NSRWT performs better than other methods followed closely by PCA–NSST with difference of

0.0089. PCA–NSST stands second for all dataset in computing similarity based on spectral features. SSIM of PCA–NSRWT gives better result for all datasets with difference of 0.0062, 0.0041 and 0.0123 for dataset 1, 2 and 3, respectively. These indicates that the fused image obtained using PCA–NSRWT is similar and integrates most of the features from source images. SSRWT and PCA–SSRWT fail to incorporate information from source image as it suffers from visual artifacts. The fused image obtained using PCA–NSRWT has incorporated most of the information from source images and is superior to the fused images of other methods. Table 1 clearly indicates that for dataset 1, 2 and 3, PCA–NSRWT exhibits minimum error rate (MSE) than NSST which stands second in the race. For dataset 1, 2 and 3, PCA–NSRWT outperforms NSST with



Table 2 Quantitative analysis of the fused images based on similarity metrics

Dataset	Methods/parameters	SAM	UIQI	D_{λ}	D_S	QNR
Dataset 1	PCA	3.13	0.8356	0.1142	0.0980	0.7989
	DWT	2.01	0.7463	0.0159	0.0704	0.9148
	SWT	2.01	0.7891	0.0230	0.0496	0.9285
	NSCT	1.45	0.8042	0.0343	0.1229	0.8470
	NSST	2.10	0.5928	0.0990	0.1865	0.7329
	SSRWT	3.14	0.7925	0.0070	0.1902	0.8041
	NSRWT	1.45	0.9190	0.1567	0.0735	0.7804
	PCA-NSCT	1.39	0.8640	0.0847	0.0983	0.8253
	PCA-NSST	1.41	0.8194	0.0837	0.0927	0.8313
	PCA-SSRWT	2.19	0.8241	0.1112	0.1904	0.7195
	PCA-NSRWT	1.23	0.9459	0.0023	0.0193	0.9784
Dataset 2	PCA	2.19	0.8174	0.1446	0.1364	0.7387
	DWT	1.95	0.7511	0.0288	0.0518	0.9208
	SWT	1.84	0.8165	0.0540	0.0637	0.8857
	NSCT	1.33	0.8213	0.0707	0.0953	0.8407
	NSST	2.02	0.6828	0.1266	0.1032	0.7832
	SSRWT	2.98	0.6265	0.0243	0.0387	0.9379
	NSRWT	1.31	0.9328	0.0493	0.0267	0.9253
	PCA-NSCT	1.34	0.8472	0.0190	0.1176	0.8656
	PCA-NSST	1.52	0.7814	0.0362	0.0118	0.9524
	PCA-SSRWT	1.91	0.8024	0.1381	0.0321	0.8342
	PCA-NSRWT	1.20	0.9589	0.0190	0.0213	0.9583
Dataset 3	PCA	4.23	0.7402	0.1353	0.1320	0.7505
	DWT	3.20	0.6158	0.0635	0.0502	0.8894
	SWT	3.15	0.6756	0.0093	0.0491	0.9420
	NSCT	1.56	0.6924	0.0303	0.1272	0.8463
	NSST	1.99	0.5594	0.1266	0.1032	0.7832
	SSRWT	2.11	0.5169	0.0231	0.2035	0.7781
	NSRWT	1.33	0.9211	0.1639	0.0932	0.7581
	PCA-NSCT	1.37	0.8472	0.1205	0.1036	0.7883
	PCA-NSST	1.49	0.6761	0.0009	0.1202	0.8790
	PCA-SSRWT	1.89	0.8332	0.1307	0.2041	0.6918
	PCA-NSRWT	1.11	0.9341	0.0082	0.0123	0.9796

notable difference of 1.7625, 8.4012 and 29.6504, respectively.

Table 2 gives quantitative analysis for measuring spectral quality of the fused images namely SAM, UIQI, D_{λ} , D_{S} and QNR. For all data sets, PCA–NSRWT shows splendid performance as compared to other methods in preserving spectral quality of the fused images. Though visual artifacts persist in the fused image of PCA–SSRWT, spectral and spatial quality has improved more than individual SSRWT and PCA.

Table 3 gives information about the artifacts that are introduced into fused image during process of fusion. To verify false artifacts introduced during fusion process, objective image fusion performance parameters along with edge preservation metric for individual bands are used

(Jagalingam & Hegde, 2015; Xydeas & Pertrovic, 2000). Objective image fusion performance measures estimate total amount of information transferred from source image to fused image (Q_{abf}) and compute the fraction of information lost (L_{abf}) and false artifacts (N_{abf}) introduced during process of fusion. As indicated in Table 3, PCA–NSRWT retains most of the information from input MS and PAN images followed closely by NSRWT with minimum difference of 0.0008 and 0.0011 for dataset 2 and 3, respectively. For dataset 1, NSCT performs better than PCA–NSRWT with minimum difference of 0.0131. Except for dataset 3, PCA performs better than all other methods with minimum amount of data loss during fusion process. For dataset 3, PCA–NSRWT stands first with minimum information lost (i.e., 0.0238). NSCT introduces minimum



Table 3 Quantitative analysis of the fused image based on objective image fusion performance and edge preservation metrics

Data sets	Methods/Parameters Reference value	Q_{abf} close to $+ 1$	L_{abf} close to 0	N_{abf} close to 0	r band close to $+ 1$	g band close to $+ 1$	b band close to $+1$
Data set 1	PCA	0.8485	0.0349	0.1166	0.5223	0.5239	0.5267
	DWT	0.2858	0.6335	0.0807	0.4335	0.4337	0.4389
	SWT	0.3427	0.4895	0.1678	0.4940	0.4923	0.4929
	NSCT	0.8877	0.1045	0.0078	0.4541	0.4587	0.4569
	NSST	0.7152	0.2732	0.0116	0.4449	0.3883	0.4371
	SSRWT	0.8735	0.1091	0.0174	0.4780	0.4696	0.4585
	NSRWT	0.4169	0.1007	0.4823	0.6354	0.6370	0.6371
	PCA-NSCT	0.8688	0.0593	0.0719	0.5480	0.5330	0.5439
	PCA-NSST	0.8364	0.0812	0.0824	0.5718	0.5551	0.5696
	PCA-SSRWT	0.6029	0.1351	0.2620	0.5075	0.5011	0.5052
	PCA-NSRWT	0.8746	0.1090	0.0164	0.6530	0.6517	0.6526
Data set 2	PCA	0.9299	0.0305	0.0396	0.4688	0.5049	0.4710
	DWT	0.2505	0.6900	0.0596	0.4577	0.4568	0.4539
	SWT	0.2969	0.6129	0.0902	0.5050	0.4901	0.4998
	NSCT	0.9299	0.0642	0.0059	0.4476	0.4408	0.4374
	NSST	0.7428	0.2442	0.0131	0.4772	0.4883	0.4192
	SSRWT	0.6045	0.1275	0.2680	0.4973	0.5100	0.4622
	NSRWT	0.9309	0.0611	0.0081	0.6069	0.5926	0.6268
	PCA-NSCT	0.8884	0.0807	0.0309	0.5279	0.5159	0.5199
	PCA-NSST	0.7880	0.1790	0.0330	0.0.5247	0.5442	0.4702
	PCA-SSRWT	0.6876	0.1452	0.1673	0.5131	0.4996	0.4913
	PCA-NSRWT	0.9317	0.0608	0.0075	0.5995	0.5940	0.5802
Data set 3	PCA	0.9458	0.0471	0.0070	0.5086	0.5449	0.5025
	DWT	0.6805	0.1465	0.1730	0.5026	0.5056	0.4928
	SWT	0.6159	0.1300	0.2541	0.5479	0.5359	0.5390
	NSCT	0.9400	0.0546	0.0054	0.4911	0.4840	0.4645
	NSST	0.8260	0.1642	0.0098	0.5937	0.5903	0.4784
	SSRWT	0.2498	0.6916	0.0586	0.5335	0.5454	0.4875
	NSRWT	0.9467	0.0469	0.0064	0.6136	0.6093	0.5964
	PCA-NSCT	0.8996	0.0779	0.0226	0.5708	0.5564	0.5173
	PCA-NSST	0.8356	0.1382	0.0262	0.5997	0.5925	0.5279
	PCA-SSRWT	0.3009	0.6139	0.0852	0.5269	0.5250	0.5148
	PCA-NSRWT	0.9478	0.0238	0.0284	0.6310	0.6236	0.6429

amount of false artifacts during fusion. DWT and SWT show poor performance in retaining information from source images. SSRWT and PCA–SSRWT show very poor performance for the fact that both algorithms introduce visual artifacts (shifting effect and shift distortion) during fusion process.

Edge information for individual r, g and b bands of fused image is presented in Table 2. For data set 1 and 3, PCA–NSRWT successfully preserves edge information for all bands followed by NSRWT. For data set 2, PCA–NSRWT shows better performance in preserving edge information for band g, whereas NSRWT has better edge

information for bands r, b with 0.0074 and 0.0466 difference to that of PCA–NSRWT. For band g, PCA–NSRWT shows better result with difference of 0.014. Even though PCA–SSRWT suffers from visual artifacts, it stands third in the list in preserving edge information. In general, PCA–NSRWT shows better result in preserving edge information compared to other methods. Table 4 presents the time complexity in terms of execution time in seconds on average basis for all the algorithms. Though PCA–NSRWT has large average execution time than individual PCA and NSRWT, PCA–NSRWT has better spectral and spatial quality. The drawbacks (shifting effect and shift distortion)



Table 4 Execution time (seconds) of different fusion algorithms (CPU i5 2.30 GHz, RAM 8 GB, Matlab 2013a)

Methods		PCA	A DWT	SWT	NSCT	NSST
Execution ti	me	2.58	13.15	327.99	642.40	669.92
Methods	SSR	WT	NSRWT	PCA- NSCT	PCA- NSST	PCA– SSRWT
Execution Time	20.3	3	49.17	594.31	656.16	21.50
Method PCA-NSRWT						
Execution time						44

of SSRWT and PCA-SSRWT are overcome by NSRWT and PCA-NSRWT. Even though the proposed algorithm gives good result, there is still chance of improvement in spectral and spatial quality of the fused image. In future, we will be testing the proposed algorithm with images captured by various sensors, e.g., QuickBird, IKONOS, and GeoEye. Further, we also need to test the proposed algorithm by combining data from various sensors, e.g., MS image captured from Landsat-8 and PAN image from QuickBird.

On the basis of visual and quantitative analysis, it is evident that PCA–NSRWT has enhanced fused image spectrally as well as spatially. PCA–SSRWT has enhanced fused image spectrally, but it is a poor performer than PCA–NSRWT due to visual artifacts. The quantitative result advocates the visual interpretation, and it is apparent to say that among the two proposed hybrid satellite fusion algorithms, PCA–NSRWT performs better then PCA–SSRWT.

Conclusion

This paper presents two pansharpening algorithms based on standard PCA combined with rotated wavelet transform namely PCA–SSRWT and PCA–NSRWT. Visual artifacts like color distortion, shifting effect and shift distortion introduced by SSRWT and PCA–SSRWT algorithms degrade spectral and spatial quality of the fused image. The fused image obtained using NSRWT dose not show shifting effect and shift distortion, but spatial quality is degraded with improved spectral quality. To improve spatial quality by maintaining spectral quality, NSRWT is integrated with PCA (PCA–NSRWT). PCA–NSRWT not only eliminates visual artifacts but also improves spectral quality by taking advantage of NSRWT, while spatial quality of the fused image is enhanced by taking benefit of

PCA where principal component (PC₁) incorporates spatial information which is common to all the bands (r, g) and b) of MS image which is histogram matched with PAN image. The fused image generated using PCA-NSRWT is superior to that of other fusion algorithms where detail features are easily distinguishable visually. The fused image as a result of PCA-NSRWT is evaluated using various performance metrics where it outperforms not only PCA and NSRWT but also other methods. Fused image of PCA-NSRWT incorporates spectral and spatial details from source images. PCA-NSRWT shows its capability in transferring features from input images into fused image without addition of false artifacts during fusion process. PCA-NSRWT is also able to preserve almost all edge information from MS and PAN images into fused image. The quantitative investigation actively exhibits robustness of the PCA-NSRWT through various performance metrics, and the overall performance of proposed algorithms for fusing satellite images shows astounding results over other fusion algorithms. The visual and quantitative analysis shows that standard PCA works better with NSRWT than SSRWT.

Declarations

Conflict of interest The author declare that they have no conflict of interest.

References

Aiazzi, B., Alparone, L., Baronti, S., & Garzelli, A. (2002). Context-driven fusion of high spatial and spectral resolution images based on oversampled multiresolution analysis. *IEEE Transactions on Geoscience and Remote Sensing*, 40(10), 2300–2312

Aiazzi, B., Alparone, L., Baronti, S., Garzelli, A., & Selva, M. (2012). Twenty-five years of pansharpening: A critical review and new developments. In Signal and image processing for remote sensing (pp. 552–599) CRC Press.

Amolins, K., Zhang, Y., & Dare, P. (2007). Wavelet based image fusion techniques—An introduction, review and comparison. ISPRS Journal of Photogrammetry and Remote Sensing, 62(4), 249–263

Bamberger, R. H., & Smith, M. J. (1992). A filter bank for the directional decomposition of images: Theory and design. *IEEE Transactions on Signal Processing*, 40(4), 882–893

Burt, P., & Adelson, E. (1983). The Laplacian pyramid as a compact image code. *IEEE Transactions on Communications*, 31(4), 532–540

Carper, W. J., Lillesand, T. M., & Kiefer, R. W. (1990). The use of intensity-hue-saturation transformations for merging SPOT panchromatic and multispectral image data. *Photogrammetric Engineering and Remote Sensing*, 56(4), 459–467

Chavan, S. S., Pawar, A., & Talbar, S. N. (2018). Multimodality medical image fusion using non-subsampled rotated wavelet transform for cancer treatment. *International Journal of Com*putational Systems Engineering, 4(2–3), 96–105



- Chibani, Y., & Houacine, A. (2002). The joint use of IHS transform and redundant wavelet decomposition for fusing multispectral and panchromatic images. *International Journal of Remote Sensing*, 23(18), 3821–3833
- Da Cunha, A. L., Zhou, J., & Do, M. N. (2006). The nonsubsampled contourlet transform: Theory, design, and applications. *IEEE Transactions on Image Processing*, 15(10), 3089–3101
- Do, M. N., & Vetterli, M. (2005). The contourlet transform: An efficient directional multiresolution image representation. *IEEE Transactions on Image Processing*, 14(12), 2091–2106
- Easley, G., Labate, D., & Lim, W. Q. (2008). Sparse directional image representations using the discrete shearlet transform. Applied and Computational Harmonic Analysis, 25(1), 25–46
- Ehlers, M., Klonus, S., Johan Åstrand, P., & Rosso, P. (2010). Multisensor image fusion for pansharpening in remote sensing. *International Journal of Image and Data Fusion*, 1(1), 25–45
- Faragallah, O. S. (2018). Enhancing multispectral imagery spatial resolution using optimized adaptive PCA and high-pass modulation. *International Journal of Remote Sensing*, 39(20), 6572–6586.
- Garzelli, A., Nencini, F., & Capobianco, L. (2008). Optimal MMSE pan sharpening of very high resolution multispectral images. IEEE Transactions on Geoscience and Remote Sensing, 46(1), 228–236
- González-Audícana, M., Saleta, J. L., Catalán, R. G., & García, R. (2004). Fusion of multispectral and panchromatic images using improved IHS and PCA mergers based on wavelet decomposition. *IEEE Transactions on Geoscience and Remote Sensing*, 42(6), 1291–1299
- Jagalingam, P., & Hegde, A. V. (2015). A review of quality metrics for fused image. Aquatic Procedia, 4, 133–142
- Johnson, B. A., Tateishi, R., & Hoan, N. T. (2013). A hybrid pansharpening approach and multiscale object-based image analysis for mapping diseased pine and oak trees. *International Journal of Remote Sensing*, 34(20), 6969–6982
- Kim, S. D., & Udpa, S. (2000). Texture classification using rotated wavelet filters. IEEE Transactions on Systems, Man, and Cybernetics-Part A: Systems and Humans, 30(6), 847–852
- Kingsbury, N. (1999). Image processing with complex wavelets. Philosophical Transactions of the Royal Society of London A: Mathematical, Physical and Engineering Sciences, 357(1760), 2543–2560
- Labate, D., Lim, W. Q., Kutyniok, G., & Weiss, G. (2005). Sparse multidimensional representation using shearlets. In Wavelets XI, International Society for Optics and Photonics (Vol. 5914, p. 59140U).
- Laben, C. A., & Brower, B. V. (2000). Process for enhancing the spatial resolution of multispectral imagery using pan-sharpening. US Patent 6,011,875.
- Ling, Y., Ehlers, M., Usery, E., & Madden, M. (2008). Effects of spatial resolution ratio in image fusion. *International Journal of Remote Sensing*, 29(7), 2157–2167
- Li, H., Manjunath, B., & Mitra, S. K. (1995). Multisensor image fusion using the wavelet transform. *Graphical Models and Image Processing*, 57(3), 235–245
- Liu, X., Wang, Y., & Liu, Q. (2018). PSGAN: A generative adversarial network for remote sensing image PAN-sharpening. In 2018 25th IEEE international conference on image processing (ICIP) (pp. 873–877). IEEE.
- Ma, J., Yu, W., Chen, C., Liang, P., Guo, X., & Jiang, J. (2020). Pan-GAN: An unsupervised learning method for pan-sharpening in remote sensing image fusion using a generative adversarial network. *Information Fusion*, 62, 110-120.

- Ma, J., Yu, W., Liang, P., Li, C., & Jiang, J. (2019). FusionGAN: A generative adversarial network for infrared and visible image fusion. *Information Fusion*, 48, 11–26
- Mallat, S. G. (1989). A theory for multiresolution signal decomposition: The wavelet representation. *IEEE Transactions on Pattern Analysis and Machine Intelligence*, 11(7), 674–693
- Mangolini, M. (1994). Contribution of pixel-based multi-sensor satellite image fusion in remote sensing and photo-interpretation. PhD Thesis, University of Nice Sophia-Antipolis
- Masi, G., Cozzolino, D., Verdoliva, L., & Scarpa, G. (2016).Pansharpening by convolutional neural networks. *Remote Sensing*, 8(7), 594
- Nason, G. P. & Silverman, B. W. (1995). The stationary wavelet transform and some statistical applications. In *Wavelets and* statistics (pp. 281–299). Springer.
- Nunez, J., Otazu, X., Fors, O., Prades, A., Pala, V., & Arbiol, R. (1999). Multiresolution-based image fusion with additive wavelet decomposition. *IEEE Transactions on Geoscience and Remote Sensing*, 37(3), 1204–1211
- Palsson, F., Sveinsson, J. R., Ulfarsson, M. O., & Benediktsson, J. A. (2016). Quantitative quality evaluation of pansharpened imagery: Consistency versus synthesis. *IEEE Transactions on Geoscience and Remote Sensing*, 54(3), 1247–1259
- Pohl, C., & Van Genderen, J. L. (1998). Review article multisensor image fusion in remote sensing: Concepts, methods and applications. *International Journal of Remote Sensing*, 19(5), 823–854
- Pohl, C., & Van Genderen, J. L. (2016). Remote sensing image fusion: A practical guide. CRC Press
- Pradhan, P. S., King, R. L., Younan, N. H., & Holcomb, D. W. (2006). Estimation of the number of decomposition levels for a wavelet-based multiresolution multisensor image fusion. *IEEE Transactions on Geoscience and Remote Sensing*, 44(12), 3674–3686
- Shah, V. P., Younan, N. H., & King, R. L. (2008). An efficient pansharpening method via a combined adaptive PCA approach and contourlets. *IEEE Transactions on Geoscience and Remote* Sensing, 46(5), 1323–1335
- Vicinanza, M. R., Restaino, R., Vivone, G., DallaMura, M., & Chanussot, J. (2015). A pansharpening method based on the sparse representation of injected details. *IEEE Geoscience and Remote Sensing Letters*, 12(1), 180–184
- Vivone, G., Alparone, L., Chanussot, J., Dalla Mura, M., Garzelli, A., Licciardi, G. A., Restaino, R., & Wald, L. (2015). A critical comparison among pansharpening algorithms. *IEEE Transac*tions on Geoscience and Remote Sensing, 53(5), 2565–2586
- Wald, L. (1999). Some terms of reference in data fusion. *IEEE Transactions on Geoscience and Remote Sensing*, 37(3), 1190–1193
- Xu, H., Ma, J., Shao, Z., Zhang, H., Jiang, J., & Guo, X. (2021). SDPNet: A deep network for pan-sharpening with enhanced information representation. *IEEE Transactions on Geoscience* and Remote Sensing, 59(5), 4120–4134.
- Xydeas, C., & Petrovic, V. (2000). Objective image fusion performance measure. *Electronics Letters*, 36(4), 308–309
- Yang, J., Fu, X., Hu, Y., Huang, Y., Ding, X., & Paisley, J. (2017).
 PanNet: A deep network architecture for pan-sharpening. In Proceedings of the IEEE International Conference on Computer Vision (pp. 5449–5457).
- Zhang, H. K., & Huang, B. (2015). A new look at image fusion methods from a Bayesian perspective. *Remote Sensing*, 7(6), 6828–6861



- Zhang, K., Zhang, F., & Yang, S. (2019). Fusion of multispectral and panchromatic images via spatial weighted neighbor embedding. *Remote Sensing*, 11(5), 557
- Zhang, Y., & Hong, G. (2005). An IHS and wavelet integrated approach to improve pan-sharpening visual quality of natural colour IKONOS and QuickBird images. *Information Fusion*, 6(3), 225–234
- Zhong, S., Zhang, Y., Chen, Y., & Wu, D. (2017). Combining component substitution and multiresolution analysis: A novel

generalized BDSD pansharpening algorithm. *IEEE Journal of Selected Topics in Applied Earth Observations and Remote Sensing*, 10(6), 2867–2875

Publisher's Note Springer Nature remains neutral with regard to jurisdictional claims in published maps and institutional affiliations.

